

Ultrastructural & mechanical characterisation of the elastic fibre network in the human annulus fibrosus

By

Vy Nguyen Khanh Bui

*Thesis
Submitted to Flinders University
for the degree of*


Master of Biomedical Engineering
College of Science and Engineering
22/5/2023

SUPERVISORS: ASSOCIATE PROFESSOR JOHN COSTI

Declaration

I certify that this thesis:

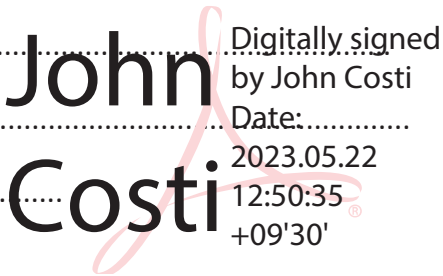
1. does not incorporate without acknowledgment any material previously submitted for a degree or diploma in any university
2. and the research within will not be submitted for any other future degree or diploma without the permission of Flinders University; and
3. to the best of my knowledge and belief, does not contain any material previously published or written by another person except where due reference is made in the text.

Signature of student.....

Print name of student.....Vy Bui.....

Date.....22/05/2023.....

I certify that I have read this thesis. In my opinion it is/is not (please circle) fully adequate, in scope and in quality, as a thesis for the degree of Master of Biomedical Engineering. Furthermore, I confirm that I have provided feedback on this thesis and the student has implemented it minimally/partially/fully (please circle).

Signature of Principal Supervisor..... Digitally signed

Print name of Principal Supervisor..... John Costi Date:.....

Date..... 2023.05.22 12:50:35 +09'30'

Executive Summary

Disc degeneration is a condition that leads to low back pain, which is a serious health risk and carries major societal and economic impact. Disc degeneration occurs as a result of changes within the intervertebral disc (IVD), mainly a decrease in the structural integrity of the IVD's components. The interlamellar matrix (ILM) has been shown to affect the mechanical properties of the IVD. Elastic fibres (EF) are an important component of the interlamellar matrix, however the details of their contribution to the behaviour of the ILM and the overall annulus fibrosus have not been specified.

This study aims to improve the technique to isolate elastic fibres from the other components of the ILM, allowing for mechanical testing of the EF network. The process involves alkaline treatment using sonication, followed by heat treatment. Results were verified using scanning electron microscopy. An attempt in mechanical testing was also carried out on partially digested samples.

Several factors that may affect the outcome of the digestion protocol were investigated, and an improvement in EF visualisation was achieved. Transition to the mechanical testing phase was deemed possible, although actual tests carried out during this project yielded unsatisfactory results. Further testing is required to fully optimise the digestion protocol and verify that it can be reliably practiced on human ILM samples.

Acknowledgements

I would like to thank Associate Professor John Costi for guiding me proceed throughout my project, and for Dr. Javad Tavakoli for providing me with advise regarding the digestion process.

I would also like to thank Mr. Rory Daniel for training me though different steps of the digestion protocol.

I would also like to thank Mr. Michael Russo for helping me with sample preparation and operation of the CellScale tester. I would like to acknowledge Ms. Ushmita Reebye who introduced me to the micro-mechanical testing process.

Finally, I would like to thank Dr. Alex Sibley for training me to use the scanning electron microscope, and Ms. Pat Vilimas for assisting me in the use of the cryostat microtome.

Table of Contents

Declaration.....	2
Executive Summary.....	3
Acknowledgements	4
Chapter I: Introduction	7
1. Low back pain and disc degeneration	7
2. Intervertebral disc components	7
3. The interlamellar matrix and its composition	9
4. Isolation of elastic fibres	10
5. Aim	13
Chapter II: Methodology.....	14
1. Sample preparationc	14
a) Hand microtome sectioning.....	15
b) Cryostat microtome sectioning.....	15
2. Sample holder and stand.....	16
3. Digestion protocol.....	17
4. SEM imaging.....	18
5. Micromechanical testing	19
Chapter III: Results.....	22
1. Digestion protocol.....	22
2. Mechanical testing	28
Chapter IV: Discussion	30
1. Identification of EF within areas of interest.....	30
2. Digestion protocol.....	31
a) Hand microtome sectioning.....	32
b) Effects of different parameters on digestion results	33
c) SEM imaging quality.....	36
d) Effects of the digestion process on 3D printed apparatuses	37
e) Mechanical testing	38
Chapter V: Future Work.....	40
Chapter VI: Conclusion.....	42
Bibliography	43
Appendices	46
Methodology	46

Tables and Figures

Figure 1: Structure of the intervertebral disc (Raj, 2008)8

Figure 2: Visualisation of elastic fibre network in ovine ILM (Tavakoli et al., 2017).10

Figure 3: Elastic fibres in human ILM as imaged by Herath.12

Figure 4: Elastic fibres in human ILM as visualised by Daniel.12

Figure 5: Digestion protocol and mechanical testing on human ILM elastic fibre project procedures.....14

Figure 6: Sample preparation for EF isolation procedure, using the cryostat microtome method. a) Isolated intervertebral disc with anterolateral section extracted. b) Section was attached to the cryostat microtome via OCT. Note that the platform could be adjusted so that it tilted forward, allowing for oblique cuts to be made. c) 4 samples were placed inside the sample holder.15

Figure 7: 3D model of a) the top half of the sample holder and b) stand, showing: 1) a meshed slot used to keep sample in place while still allowing vibrations and liquid to permeate, 2) circular slot for insertion of stand, 3) mark to identify holder direction.....16

Figure 8: Setup for the sonication process. a) A sample holder placed on stand and weighed down using a stainless screw. b) Sample stand placed inside NaOH solution, directly beneath the sonicator’s nozzle (1). The distance between the holder top and tip of nozzle was 45 cm.17

Figure 9: Sample holder placed inside chamber before imaging.18

Figure 10: Micromechanical test setup for a) tensile (radial) loading; b) shear (circumferential) loading. Also pictured: close-ups of specimen during tensile testing at c) 0% stretch and d) 40% stretch; and close-ups of specimens during shear testing at e) 0% stretch and f) 40% stretch. ILM is highlighted in red.20

Figure 11: Elastic fibre network detected in a sample sonicated in 1M NaOH for 120 minutes at the magnification of a) 3,000 and b) 6,00026

Figure 12: Elastic fibre network detected in a sample sonicated in 1M NaOH for 60 minutes, with nozzle placed closer to surface of holder.27

Figure 13: Mechanical test results for tensile testing, presented as a) a force-displacement plot and b) force-time plots for all sessions. Shear test results are also shown as c) a force-displacement plot and d) force-time plots for all sessions.29

Figure 14: Undigested surface texture at a) 12,000 magnification, and b) 80,000 magnification, showing banding in fibres. c) A tear, with parallel ridges possibly indicating lamella-ILM boundary.31

Figure 15: Comparison between Dr. Tavakoli's ovine ILM results, Daniel's human ILM results, and this project's best outcome.32

Figure 16: Possible explanation for the interaction between ultrasonic waves and sample holders at different distances to nozzle.....35

Figure 17: Qualitative comparison to digest ILM's behaviour in ovine discs. Left side: partially digested human ILM. Right side: normalised digested ovine ILM results (Javad Tavakoli & John J. Costi, 2018b). Both were tested using the same strain rates.38

Chapter I: Introduction

1. Low back pain and disc degeneration

Low back pain is a condition that's defined by pain around the inferior portion of the spine. It varies in severity, from mild symptoms to prolonged, chronic pains (Nepomuceno & Turra, 2015). Many patients report significant impact on their quality of life, citing that lower back pain inhibits their work performance, which in turn leads to job dissatisfaction and insecurity, and causes significant physical and psychological impacts such as stress, anxiety, depression (Hoy et al., 2010). It was found that the condition occurs in 80% of adults at one point in their life within Australia (Walker et al., 2004); globally, it is cited as the leading cause of disability, peaking in ages between 35 and 50 (Damian et al., 2014). Because of its prominence, low back pain has become a significant societal and economic burden, especially to aging populations and in low-income communities. There is an urgent need for attention and recognition of the condition, as well as a push for scientific research into its mechanism and care strategies (Buchbinder et al., 2018).

One of the physiological processes that was found to directly lead to low back pain is degenerative disc disease, or disc degeneration. It is generally understood as a series of symptoms affecting the structural integrity of the intervertebral disc that is brought on by aging and overuse from repetitive activities. As aging and injuries progress, several effects can be seen occurring to the disc, namely a loss of water, damages to the collagen network, and inhibition of disc repairs (Adams & Roughley, 2006). These, along with genetic factors (Livshits et al., 2011), further lead to a number of failures in the disc components.

2. Intervertebral disc components

The intervertebral disc (IVD) consists of three components (Figure 1). The nucleus pulposus (NP) is the gelatinous substance that lies at the core of the disc. It consists of mostly water and proteoglycans, at approximately 77% and 14% of wet weight respectively. With proteoglycans being a type of protein consisting of water-retaining chains called glycosaminoglycans (GAGs), this composition signifies hydrostatic pressures as its primary mechanical feature (Alonso & Hart, 2014). The NP is surrounded by fibrocartilaginous sheets of lamellae making up what is called the annulus fibrosus (AF). The lamellae of the AF is made of type I collagen fibres arranged in concentric layers, alternating in directions at 30° – 44°

(Marcolongo et al., 2017) to the transverse plane. This structure gives the IVD a tougher exterior which aids its ability to resist the pressurized swelling of the NP (Adams & Dolan, 2015) and primarily contributes to the disc's anisotropic behaviour (Baldit, 2018). The AF and NP are then supported by the vertebral endplate (VEP), which is a bilayer structure that acts as the interface between the IVD and vertebral column, separating the disc from the bone.

Figure removed due to copyright restriction.

FIGURE 1: STRUCTURE OF THE INTERVERTEBRAL DISC (RAJ, 2008)

The purpose of the IVD is to separate adjacent vertebral columns and allow 6 degree-of-freedom movement of the spine, with some studies suggesting a distribution of stresses and shock absorption as other important roles (Inoue & Takeda, 1975). Disruption of IVD structure can be caused by the gradual depletion of water content through and enhanced by the loss of water-retaining GAGs. These losses mean that tissue swelling is compromised, leading to a decrease in disc volume and pore size which affects tissue permeability (Baltoni & Gu, 2019). Inhibition of substance transport, along with a depletion of nutrients that come with age and injury-related metabolic activities, give rise to structural breakdown and problematic biological performances. The disc becomes stiff. Stresses are distributed unevenly across the disc surface, from which pathological symptoms correlating to low back pain arise.

Among the various manifestations of disc degeneration, disc herniation is the most recognisable. As the AF experiences rupture due to the aforementioned structural breakdown, spinal loading is exerted upon the NP, pushing the material to extrude outwards. Extruded NP leans against the spinal cord, causing inflammation and pain (Guterl et al., 2013). Ruptures in the AF are known as annular tears, which is another symptom of disc degeneration, and often

occur in affected discs as a result of structural wear and tears. Pain thus arises from ingrowth of nerve endings and granulation tissue between tears (Fletcher et al., 2002; Tenny & Gillis, 2023).

The AF plays an important role in governing the mechanical behaviour of the IVD, allowing the disc to withstand complex loads exerted by spinal movements. Mechanical behaviour can be inferred to involve the contribution of not only the collagen-rich lamellar components, but also the interlamellar matrix (ILM) that acts as an adhesive between them. Compressive stresses exerted on the IVD translates to radial fluid pressures exerted on the AF walls and in turn, the ILM, while rotational motion directly relates to circumferential stresses experienced by the ILM. Repeated loading on the ILM leads to the separation between AF layers, also known as delamination, which is an important source of disc degeneration, as previously established (Tavakoli et al., 2016).

3. The interlamellar matrix and its composition

The ILM is approximately 30 μm thick and consists of proteoglycans arranged in a complex network of cross-bridges, elastic fibres, and other proteins (Tavakoli et al., 2016). Elastic fibres (EF) are thin fibres of under 2 μm in thickness, occupying 2% of the IVD's total dry weight. They appear in various connective tissues of the body such as skin, arteries, and ligaments, and are made of an elastic core surrounded by fibrillin-based microfibrils (Kielty et al., 2002). Their role is to provide these tissues with elastic recoil and resilience against deformity (Lannoy et al., 2014). It can be generally assumed that elastic fibres in the ILM exhibit similar elasticity, and it was found that the elastin content increased with degenerated discs (Cloyd & Elliott, 2007); however, there is still insufficient knowledge regarding the specifics of such behaviour and its effect on the overall properties of the IVD.

The mechanical behaviour of the ILM as a whole has been examined in a few research papers. A study was carried out to visualise the elastic fibres within the ILM of ovine samples (Tavakoli et al., 2017), and is displayed in Figure 2. Another was done on the mechanical properties of ovine ILM via tensile tests (Mengoni et al., 2015), showing higher stiffness in the outer lamellae compared to the inner lamellae. Pezowicz et al. carried out radial and tangential stretch tests on bovine slices in order to investigate interlamellar cohesion (Pezowicz et al.,

2006). Peel tests were conducted on degenerated human IVDs to obtain delamination strengths for different regions of AF at various rates (Gregory et al., 2012).

Research has also been done on the elastic fibres, however the number of published papers is still limited with regards to their mechanical characteristics within the ILM. The presence of elastic fibres has been quantified for bovine tail (Yu et al., 2002). Iatridis et al. found that damages to the AF structure greatly affect the ILM region through tensile testing (Smith & Fazzalari, 2009). Shear tests were performed on bovine samples to confirm the effect of the elastic fibre network (Michalek et al., 2009). Tavakoli and Costi managed to isolate the elastic fibre network in ovine disc ILM and measured its mechanical properties (Tavakoli & Costi, 2018c). No such tests have been done on elastic fibres of human ILM. This is due to the lack of a reliable method to isolate EF in human.

Figure removed due to copyright restriction.

FIGURE 2: VISUALISATION OF ELASTIC FIBRE NETWORK IN OVINE ILM (TAVAKOLI ET AL., 2017).

4. Isolation of elastic fibres

Various methods of isolating elastic fibres have been employed in different papers. Miller and Fullmer used guanidine homogenization on aortas, then treated them with collagenase, which is an enzyme that can break down collagens (Miller & Fullmer, 1966). This technique was later adopted and applied on pulverized ligaments in several studies (Daamen et al., 2005; John & Thomas, 1972; Ross & Bornstein, 1969). In another, bovine samples were treated with

hyaluronidase to partially digest GAGs, then with collagenase to remove collagen, and underwent orcein staining solution and immunostaining so they can be visualised using light microscopy (Yu et al., 2002). While this approach is promising in theory, enzymatic treatment is complicated, costly, and can cause over-digestion in delicate samples.

Another digestion method is using alkaline to purify elastin, first proposed by Lansing et al. (Lansing et al., 1952). This method was then replicated in successive studies for different connective tissues (Gotte et al., 1963; Pierce & Ebert, 1965). John and Thomas used an alkaline solution heated to high temperatures in their treatment of pulmonary tissues (John & Thomas, 1972), and the modified protocol, known as hot alkaline extraction, was adapted by later studies (Keeley & Partridge, 1974; Long & Tranquillo, 2003). These procedures involved saline treatment and pulverisation of samples, and elastin content was quantified using appropriate analysers. Thus, they would be inappropriate for samples that require subsequent testing.

Sonication was suggested to speed up the alkali digestion process (Crissman & Pakulski, 1984; Gotte et al., 1974), as it was found to be an effective method to loosen fibrous structures. Tissues would be subjected to low-frequency ultrasonic vibrations that break off biological bonds, as seen in tissue treatment processes such as decellularization (Azhim et al., 2013; Lin et al., 2021) and fibre extraction (Gylseth et al., 1982).

Tavakoli and Costi (Tavakoli & Costi, 2018a) proposed alkali digestion along with sonication at room temperature for easy preparation of AF samples. The procedure was introduced as a cost-effective alternative to traditional alkaline treatment. It was performed on ovine discs and allowed the elastin fibre network to be clearly observed under scanning electron microscopy (SEM). However, the results could not be replicated in human IVDs in a reliable manner.

Figure removed due to copyright restriction.

FIGURE 3: ELASTIC FIBRES IN HUMAN ILM AS IMAGED BY HERATH.

Herath (Herath, 2021) first attempted to visualise human EF by modifying Dr. Tavakoli's protocol as part of her research on elastic fibre isolation in both ovine and human ILM. By sonicating samples in 1M of sodium hydroxide (NaOH) for 90 minutes and 120 minutes, SEM images of the EF network were obtained, as seen in Figure 3. The number of identified fibres were limited, however.

Figure removed due to copyright restriction.

FIGURE 4: ELASTIC FIBRES IN HUMAN ILM AS VISUALISED BY DANIEL.

Following up from Herath's results, Daniel (Daniel, 2021) continued to optimise the digestion method on human ILM. A number of tests were done using different sonication parameters, and during the later stage, a technique that made sample handling much easier was introduced. The incorporation of 3D printed sample holders to store and transport samples

through all steps of the digestion and imaging process helped prevent delicate samples from being subjected to unwanted forces and damages during handling. Results obtained were correspondingly improved (Figure 4, with increased consistency across sessions. Despite this step forward, a definitive, reliable protocol to isolate EF has not been established.

5. Aim

The aim of this project is to improve on the adaptation of Dr. Tavakoli's digestion method so that a reliable, repeatable protocol to isolate elastic fibres in human ILM can be achieved. The secondary goal is to apply the protocol on human ILM and perform tension-shear tests on processed samples. Results obtained from the research will contribute to the knowledge of IVD mechanical properties and disc degeneration. It will also help expand the research into developing IVD models and treatment for low back pain.

Chapter II: Methodology

There are two stages of this project, as demonstrated in Figure 5. The first stage involved the digestion protocol itself, which was repeated with parameters altered one at a time and changes to results recorded. The second stage involved the micromechanical testing of digested samples, and was merely supplemental, as it depended entirely on a successful outcome of the previous stage.

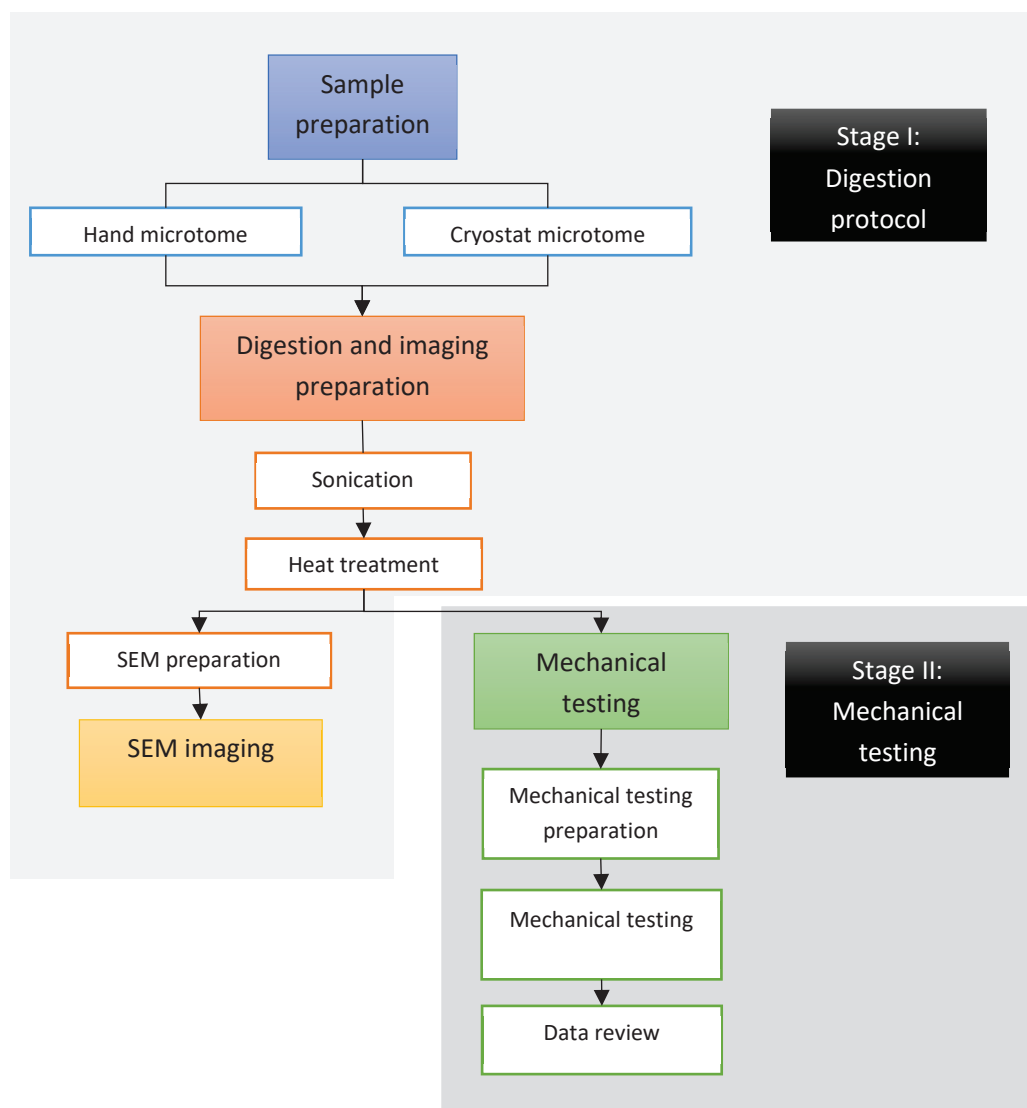


FIGURE 5: DIGESTION PROTOCOL AND MECHANICAL TESTING ON HUMAN ILM ELASTIC FIBRE PROJECT PROCEDURES.

1. Sample preparation

4 isolated, non-degenerated human intervertebral discs were kept frozen at -20°C prior to usage. Among them, 3 were extracted from lumbar FSUs (L1/L2), and 1 was from thoracic FSU

(T10/T11). Trapezoidal sections of roughly 1-1.5 cm in width were extracted from the anterior, lateral, and anterolateral regions of the annulus fibrosus. Sections were separated from the disc using a scalpel so that all AF layers were included, up to 5 mm into the NP core (Figure 6a).

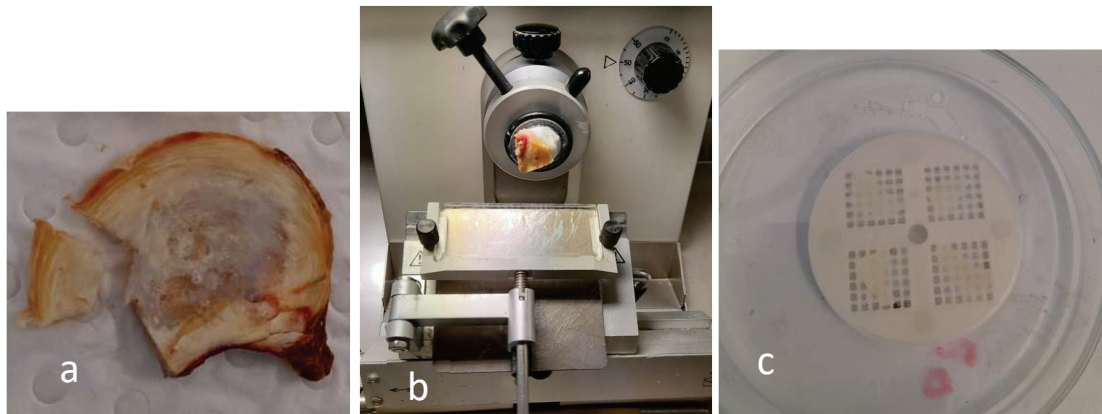


FIGURE 6: SAMPLE PREPARATION FOR EF ISOLATION PROCEDURE, USING THE CRYOSTAT MICROTOME METHOD. A) ISOLATED INTERVERTEBRAL DISC WITH ANTEROLATERAL SECTION EXTRACTED. B) SECTION WAS ATTACHED TO THE CRYOSTAT MICROTOME VIA OCT. NOTE THAT THE PLATFORM COULD BE ADJUSTED SO THAT IT TILTED FORWARD, ALLOWING FOR OBLIQUE CUTS TO BE MADE. C) 4 SAMPLES WERE PLACED INSIDE THE SAMPLE HOLDER. NOTE THAT THE DIRECTION MARKER IS PLACED UPWARDS.

a) Hand microtome sectioning

Each section was attached to a grooved platform using an O.C.T. compound (TissueTek® by Sakura FineTek, with a solidifying temperature threshold of -10°C) as an adhesive. The platform was lowered into a handheld microtome (Westlab, with the smallest division of $10\ \mu\text{m}$) and clamped into place. Cuts of 0.3 mm and 0.5 mm were attempted using a chilled razor. This process was proven to be greatly challenging and with a low success rate, producing only 12 workable slices. The slices were placed into 3 3D printed sample holders (2 containing 0.5 mm slices only, the other one containing 0.3 mm slices only), ready for digestion.

b) Cryostat microtome sectioning

Sections were brought to the Flinders Medical Centre for microtome cutting in a soft Esky cooler and kept cold using ice gel packs. They were attached to specimen discs using O.C.T. and secured within a step motor-controlled platform of a Leica® Cryocut CM1850 microtome (Figure 6b). Slices were obtained by cutting along the transverse plane of the disc with the attached blade as the specimen was kept frozen at -20°C . Slices without visible surface tears were selected and placed inside sample holders, with 4 slices per holder (Figure 6c). Each

cryotome session produced 24 – 28 slices that were used for digestion, or 6 – 7 sample holders, totalling at 5 sessions throughout the study. Slice thickness was first kept at 30 μm , then was increased to 50 μm . In the latest session, the platform was tilted downwards so that the disc section was angled at 10° from the transverse plane, allowing for oblique cuts to be made. 12 slices were produced with this arrangement. Holders were transported to Tonsley facility and stored at -20°C until digestion.

2. Sample holder and stand

The protocol employed the use of 3D printed sample holders (Figure 7a). The holders were designed by Daniel and was modified to fit the purpose of this project. Each holder consists of two circular halves, each 1 mm in thickness and was then increased to 2.5 mm to resist against the alkaline solution's corrosive effect. Four meshed slots were incorporated to accommodate four samples per digestion while still allowing liquid permeability. Gaps of 0.5 mm were left between the top and bottom meshes in each slot to prevent the samples from being compressed. Four depressions were incorporated into the bottom half to allow for easy separation, as samples may need to be extracted for mechanical testing.

The stand (Figure 7b) was also designed by Daniel. It allowed the sample holder to be lowered into and lifted from the beaker using forceps. When placed, the bottom of the sample holder would be positioned at a height of 20 mm from the bottom of the beaker. Both holder and stand were printed using the Ultimaker® 2+ 3D printer, with the minimum wall thickness of 0.4 mm. The material was Polylactic Acid (PLA).

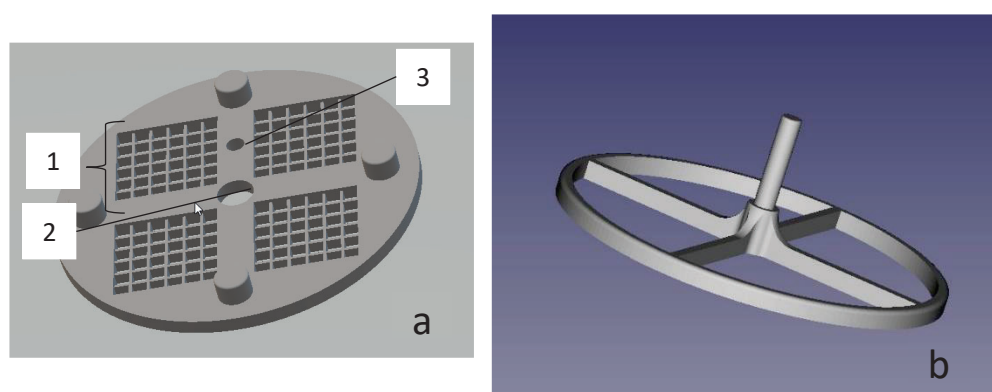


FIGURE 7: 3D MODELS OF A) THE TOP HALF OF THE SAMPLE HOLDER AND B) STAND, SHOWING: 1) A MESHED SLOT USED TO KEEP SAMPLE IN PLACE WHILE STILL ALLOWING VIBRATIONS AND LIQUID TO PERMEATE, 2) CIRCULAR SLOT FOR INSERTION OF STAND, 3) MARK TO IDENTIFY HOLDER DIRECTION.

3. Digestion protocol

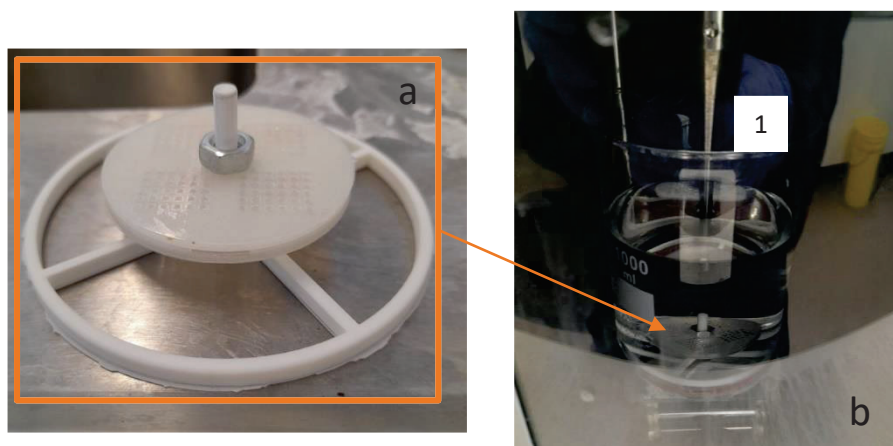


FIGURE 8: SETUP FOR THE SONICATION PROCESS. A) A SAMPLE HOLDER PLACED ON STAND AND WEIGHED DOWN USING A STAINLESS SCREW. B) SAMPLE STAND PLACED INSIDE NaOH SOLUTION, DIRECTLY BENEATH THE SONICATOR'S NOZZLE (1). THE DISTANCE BETWEEN THE HOLDER TOP AND TIP OF NOZZLE WAS 45 CM.

One sample holder was chosen for each digestion session. The sample holder was placed on the sample stand and secured with 1 – 2 stainless steel screws (Figure 8a). The screws kept the holder from floating upward and weighed down the stand. The stand was lowered into 700 ml of NaOH solution, the molarity of which was varied between sessions. The beaker was then placed under the nozzle of an MRC® 950W Ultrasonic Processor (Figure 8b). In the original setup, the nozzle's tip would be 45 cm from the surface of the sample holder. In certain sessions, the beaker was placed atop a platform that brings the nozzle to 20 cm from the sample holder.

The samples were sonicated at 25 kHz for a determined amount of time. Then, the holder was submerged in 500 ml of distilled water at room temperature for 5 minutes to rinse off the remaining chemicals. It was then placed inside 200 ml of distilled water heated to 70°C inside a laboratory oven (Labec® Horizontal Air Flow Oven) to get rid of loose collagen fibres for 15 minutes.

The holder was then placed in 100 ml of 30% ethanol for 2 minutes, then 100 ml of 70% ethanol for 2 minutes, and finally 100 ml of 90% ethanol for 30 seconds. This was done in order to dry out the surface of the samples to prepare for SEM visualisation. Afterwards, the sample holder was kept inside a vacuum oven (Labec® Vacuum Drying Ovens, coupled to an ELA-PVO 240 V pump) at 37°C and -80 kPa overnight (5 – 8 hours), further dehydrating the samples, as water molecules can negatively affect the quality of SEM images.

The parameters that were adjusted were sonication time, NaOH molarity, distance to nozzle, and heat treatment specifications. Samples also varied from each other by slice orientation and thickness.

4. SEM imaging

After drying, the vacuum oven chamber was vented and the sample holder was immediately wrapped in cling wrap, then brought to the SEM facility (Bedford Park). A metal stub was attached to the back of the holder using double-sided carbon tape. The holder was placed inside an EmiTech® K75X Sputter Coater such that it was centred on top of the spinning stage. The coater covered the surface of the holder with a 10 nm layer of platinum on each side to allow conductivity with the electron beam. Once done, the holder was carefully covered to prevent contamination as it was moved to the SEM.



FIGURE 9: SAMPLE HOLDER PLACED INSIDE CHAMBER BEFORE IMAGING.

The instrument used was an Inspect F-50 SEM (by Elecmi®). The holder was placed inside the vacuum chamber (Figure 9), and the chamber was pumped until the internal pressure reached below 10^{-2} kPa. The samples were imaged using a 5 kV high voltage beam, with a spot size of 3.

Regions where fibrous textures could be detected and tears within the surface of each sample were focused on. Undigested surfaces appeared solid at the magnification of 500 and below, and as a dense structure of thick, banded collagen fibres. Elastic fibres were identified as thin

strands of various orientations, either curled or stretched as part of an intricate network. There should be no banding on their surface to distinguish them from collagen fibres.

5. Micromechanical testing

Some micromechanical testing sessions were attempted on partially-digested samples (using 1M NaOH solution and sonicated for 120 minutes). Digested samples were extracted from the holder after heat treatment and placed inside a phosphate-buffered saline (PBS) solution at room temperature. Each sample was slid onto a glass slide and was left to dry for 2 minutes. Then, waterproof sandpaper (P400 grit) was bonded to the sample in one of two orientations (radial and circumferential) using superglue (Loctite®); sandpaper pieces were attached roughly 1 mm apart from each other on either end of a lamella.

The setup was loaded onto the CellScale® BioTester on the Y-axis, with sandpaper pieces carefully clamped to the actuators so that stress upon the load cell – the component that was responsible for measuring load - was kept at the minimum. The fluid chamber was filled with PBS saline and was raised so that the sample was submerged. Tests were done in this condition – hydrated samples at room temperature.

The direction of loading is demonstrated in Figure 10.

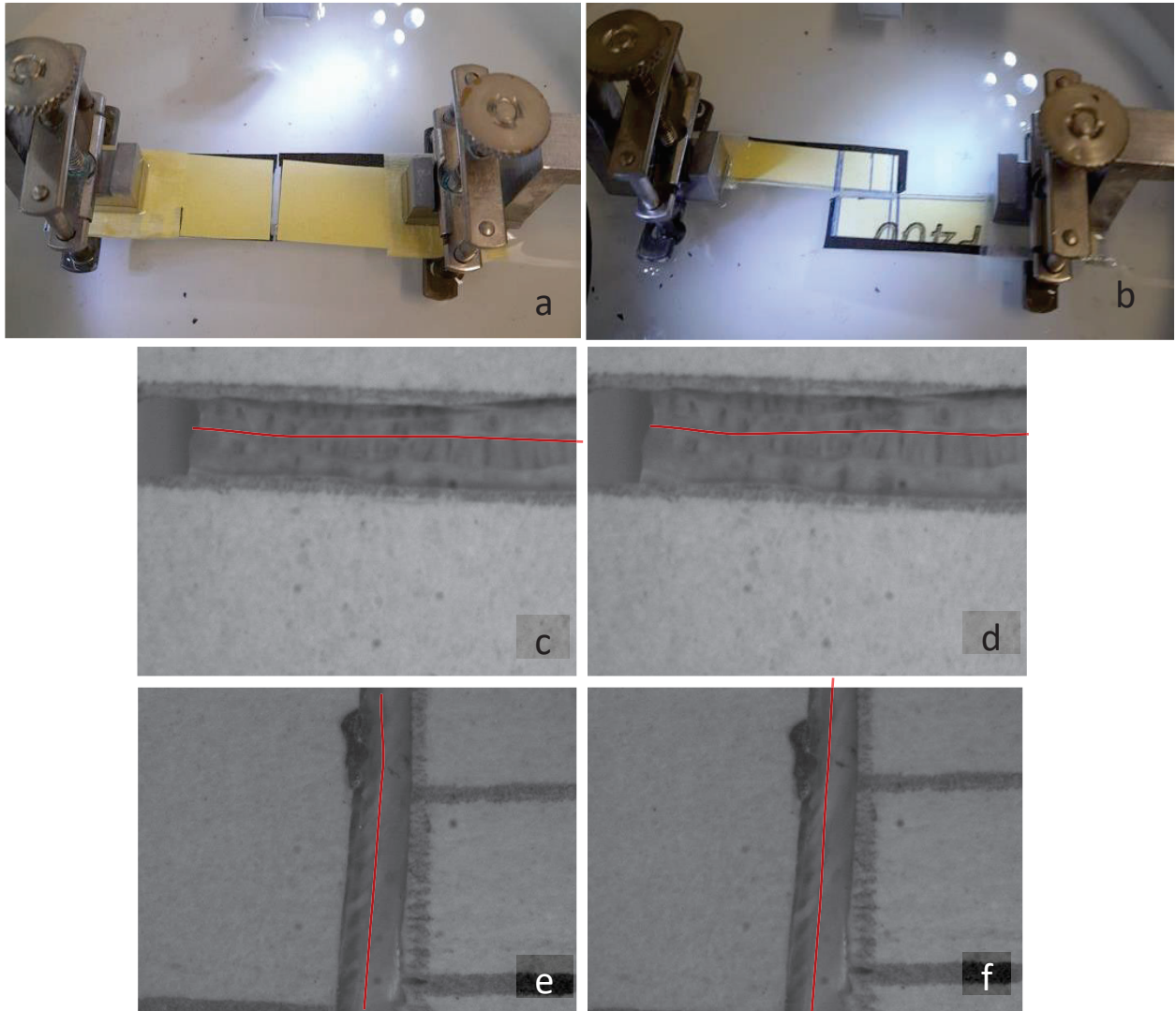


FIGURE 10: MICROMECHANICAL TEST SETUP FOR A) TENSILE (RADIAL) LOADING; B) SHEAR (CIRCUMFERENTIAL) LOADING. ALSO PICTURED: CLOSE-UPS OF SPECIMEN DURING TENSILE TESTING AT C) 0% STRETCH AND D) 40% STRETCH; AND CLOSE-UPS OF SPECIMENS DURING SHEAR TESTING AT E) 0% STRETCH AND F) 40% STRETCH. ILM IS HIGHLIGHTED IN RED.

Before each test, a preload of 100 N was applied by manually adjusting the actuators until the value was recorded by the load cell. The sample was then loaded uniaxially at three different strain rates: $1\% \text{ s}^{-1}$ (medium), $10\% \text{ s}^{-1}$ (fast), $0.1\% \text{ s}^{-1}$ (slow), until a deformation of 40% the original length (measured as the distance between opposite edges of the sandpaper pieces) was reached. The loading was repeated for three stretch-recovery cycles for each of the strain rates. Different samples were used for tensile and shear tests. Readings were plotted and images were obtained automatically using the LabJoy® software.

At the end of each session, the sample was removed from the instrument so as the load cell could be reset. This was done to ensure the accuracy of subsequent tests.

Results were exported as CSV files and plotted using MATLAB R2021a.

Chapter III: Results

1. Digestion protocol

Table 1 summarizes all attempts done during the project, along with sample specifications, test conditions, and the outcome of each session. Incidents during testing was also recorded. Overall, a total of 33 sessions were carried out, and 132 samples underwent digestion. Among them, 22 yielded notable results (a success rate of 16.67%). A sample was deemed successfully digested when an EF network was detected within its surface. Unsuccessful digestion was determined when no EF was detected, or when samples disintegrated to the point that they could not be imaged by the SEM.

TABLE 1: DIGESTION PROTOCOL TEST SESSIONS.

Session no.	Sample description	Sample thickness	Sonication time	Molarity	Nozzle distance	No. of samples that yielded notable results	Comments on failed sessions	Other comments
1	Hand microtome L1/L2 Lateral	0.3 mm	90 min	0.5 M	45 cm	1		
2	Hand microtome L1/L2 Lateral	0.5 mm	90 min	1 M	45 cm	0	Under-digested	Sample holder floated up during sonication.
3	Hand microtome L1/L2 Lateral	0.5 mm	120 min	1 M	45 cm	0	Under-digested	One sample escaped holder due to cracked mesh.
4	Cryostat microtome L1/L2 Anterior	30 μ m	90 min	0.5 M	45 cm	2		
5	Cryostat microtome ND04142-11 L1/L2 Anterior	30 μ m	90 min	1 M	45 cm (floated to the of liquid surface)	0	Under-digested	Sample holder floated to the top. Top half broke. 1 sample escaped and was successfully placed back into holder.

6	Cryostat microtome L1/L2 Anterior	50µm	90 min	1 M	45 cm (floated to ~12cm)	1		Holder floated up to 400ml mark in beaker.
7	Cryostat microtome L1/L2 Anterior	50µm	120 min	1 M	45 cm	3	Clear EF, high density	
8	Cryostat microtome L1/L2 Anterior	30µm	120 min	1 M	45 cm	0	Disintegrated	Top of holder was cracked.
9	Cryostat microtome L1/L2 Anterior	30µm	120 min	0.5 M	45 cm	2		Top of holder was cracked.
10	Cryostat microtome T10-T11 Anterolateral	30µm	90 min	1 M	12 cm	0	3 samples disintegrated 1 sample under-digested	
11	Cryostat microtome T10-T11 Anterolateral	30µm	150 min	0.5 M	45 cm	1		Stand broke halfway through, holder intact.
12	Cryostat microtome T10-T11 Anterolateral	30µm	90 min	1 M	56 cm	0		
13	Cryostat microtome T10-T11 Anterolateral	30µm	100 min	1 M	45 cm	0		
14	Cryostat microtome T10-T11 Anterolateral	30µm	100 min	1 M	45 cm	0	3 samples disintegrated. 1 sample under-digested	One sample slipped out of holder.
15	Cryostat microtome T10- T11 Anterior	50µm	120 min	0.5 M	45 cm	2		

16	Cryostat microtome T10- T11 Anterior	50µm	120 min	1 M	45 cm	0	Samples dissolved.	Parts of holder were dissolved and samples escaped.
17	Cryostat microtome T10- T11 Anterior	50µm	120 min	1 M	45 cm	0	Completely dissolved save for a few small pieces, which ended up disintegrated in hot water bath	
18	Cryostat microtome T10- T11 Anterior	50µm	90 min	1 M	45 cm	0	Samples dissolved.	
19	Cryostat microtome T10- T11 Anterior	50µm	60 min	1 M	45 cm	0	Not much digestion	
20	Cryostat microtome L1-L2 Anterolateral	50µm	150 min	0.5 M	45 cm	2		
21	Cryostat microtome L1-L2 Anterolateral	50µm	60 min	1 M	45 cm	0	Under-digested	
22	Cryostat microtome L1-L2 Anterolateral	50µm	120 min	1 M	45 cm	1		
23	Cryostat microtome L1-L2 Anterolateral	50µm	120 min	0.5 M	20 cm	1		
24	Cryostat microtome L1-L2 Anterolateral	50µm	60 min	1 M	20 cm	3		

25	Cryostat microtome L1-L2 Anterolateral	50µm	90 min	1 M	20 cm	1		
26	Cryostat microtome L1-L2 Anterolateral	50µm	120 min	1 M	20 cm	0	Disintegrated	
27	Cryostat microtome L1-L2 Anterior	50µm	120 min	0.5 M	20 cm	0	Under-digested	
28	Cryostat microtome L1-L2 Anterior	50µm	60 min	1 M	20 cm	1		
29	Cryostat microtome L1-L2 Anterior	50µm	120 min	1M	45 cm	0	Under-digested	
30	Cryostat microtome L1-L2 Anterolateral	50µm (Oblique)	90 min	1M	45 cm	0	Under-digested	
31	Cryostat microtome L1-L2 Anterolateral	50µm (Oblique)	120 min	1M	45 cm	1		
32	Cryostat microtome L1-L2 Anterolateral	50µm (Oblique)	120 min (80 degrees heat treatment)	1M	45 cm	0	Under-digested	
33	Cryostat microtome L1-L2 Anterolateral	50µm (Oblique)	120 min (18 minutes heat treatment)	1M	45 cm	0	Under-digested	

No EF network could be detected under SEM for hand microtome sectioned slices, and only the surfaces of these samples were slightly affected by digestion. Cryostat microtome sectioning was the obvious better choice to advance from Dr. Tavakoli's method, which used 30 µm slices.

30 μm slices were digested from sessions #4 - #14 (excluding sessions #6 and #7) until a thicker sample cut was pursued (50 μm). Slices with the thickness of 30 μm produced quantifiable results when a 0.5 M solution was used (#4, #9), but started to disintegrate when sonicated in 1M NaOH for 120 minutes (#5). Little digestion was seen when sonicated in 1M solution for 90 minutes (#8), which could be due to the fact that the holder floated upwards to the liquid surface and away from the nozzle. This condition was repeated (#10), and total digestion was encountered.

With 50 μm thickness, samples could withstand a higher molarity and longer sonication time, although over-digestion would sometimes occur. The best results were found in session #7 (120 minutes, 1M) (Figure 11), where fibres of under 1 μm were identified and arranged in a frazzled, web-like structure. 3 samples showed clear evidence of elastic fibres: thin, untextured strands spotted within tears that were located away from the sample's edges. Fibres could be imaged at the magnification of 3,000 up to 12,000.

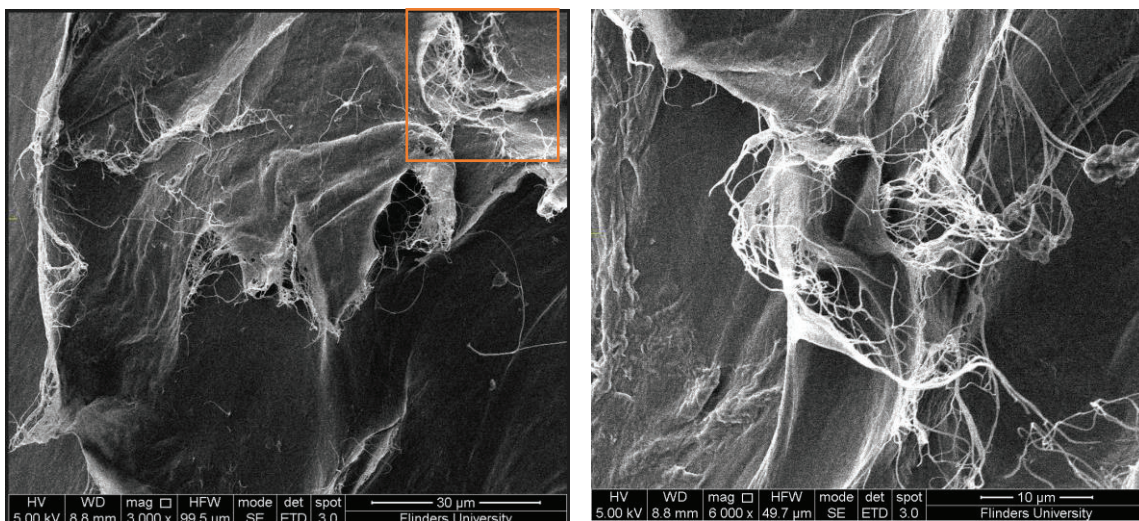


FIGURE 11: ELASTIC FIBRE NETWORK DETECTED IN SESSION #7 SONICATED IN 1M NaOH FOR 120 MINUTES AT THE MAGNIFICATION OF A) 3,000 AND B) 6,000

Subsequent tests on 50 μm samples encountered problems with the samples disintegrating, which might have tied to a change in IVD location. An attempt to vary the distance between the nozzle and the sample was done, with the sample holder either floated at the 400 ml mark, or held at the bottom of the beaker using a flat bottom stand. In both instances, the holders escaped from the intended location, and results could not be properly obtained.

Later attempts to vary the nozzle distance involved placing the beaker on top of a platform, while keeping the holder-stand setup the same inside the liquid. This allowed sample holders to be stabilised. Some decent results were obtained under this condition, however major improvement could not be identified. The best result was acquired from session #24 (60 minutes, 1M, holder placed closer to nozzle) (Figure 12). Strands of EF could be seen forming web-like structures inside tear spots. Some folding was observed which might have also contributed to the digestion capability. This condition was replicated in session #28, with less success.

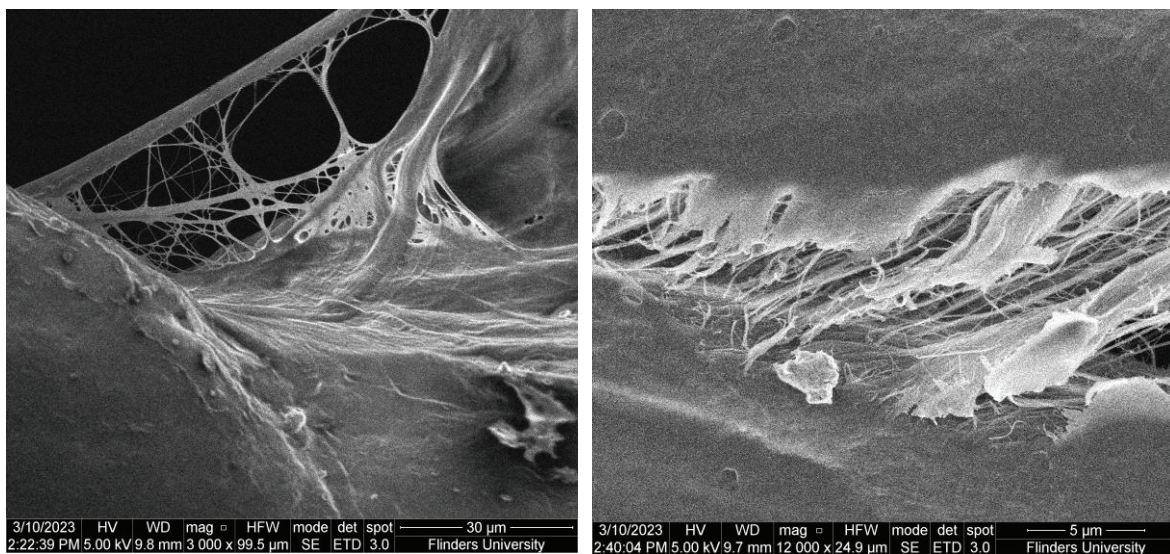


FIGURE 12: ELASTIC FIBRE NETWORK DETECTED IN SESSION #24 SONICATED IN 1M NaOH FOR 60 MINUTES, WITH NOZZLE PLACED CLOSER TO SURFACE OF HOLDER.

During several sessions, parts of the sample holder was found cracked or broken (#3, #8, #9). Meshes either broke from prolonged sonication in high molarity alkaline solution, or from proximity to the sonicator's nozzle as the holder floated up (#5). After session #9, the thickness of each holder half was increased from 1 mm to 2.5 mm to counter this problem, however they were still compromised during longer sessions.

Samples obtained from oblique cutting were tested under the same varied conditions experienced by transversely cut slices. Little improvement was observed in all but one sample (#31). Keeping the same sonication condition as #31 while varying the heat treatment parameters, results were obtained with, once again, little change.

Early sessions experienced sample holders floating upwards in the alkaline solution (#6). The most effective remedy was to use one or two stainless screws to weigh down the stand and stop the holder, which was employed from session #9 onwards.

2. Mechanical testing

Difficulties were encountered during the mechanical testing phase that caused most results to be unobtainable or unviable for analysis. First and foremost, a conclusive protocol was vital for this stage to be feasible, which was not achieved during the first stage of the project. Definitive results, therefore, were not expected during this phase. However, tests were still carried out to ensure the practicality of transitioning from the digestion stage to the mechanical testing stage.

The most common problem encountered was the destruction of samples during handling. Sample tearing could occur at any point during preparation, attachment of sample into the tester, or between test sessions. Results of the only complete procedure was recorded. Force-displacement plots of averaged values were displayed alongside raw force-time data for both tensile and shear testing (Figure 13).

The partially digested samples showed prominent hysteresis areas in all three strain rates. Errors were noticeable in all sessions, the most significant being what could have been equipment errors. At certain stresses, the load cells gave constant readings as strain increased which was most evident in the medium strain rate tests. Preloading was difficult to achieve, as the load cell readings were inconsistent, and there were multiple instances of sample failure while preloading was applied.

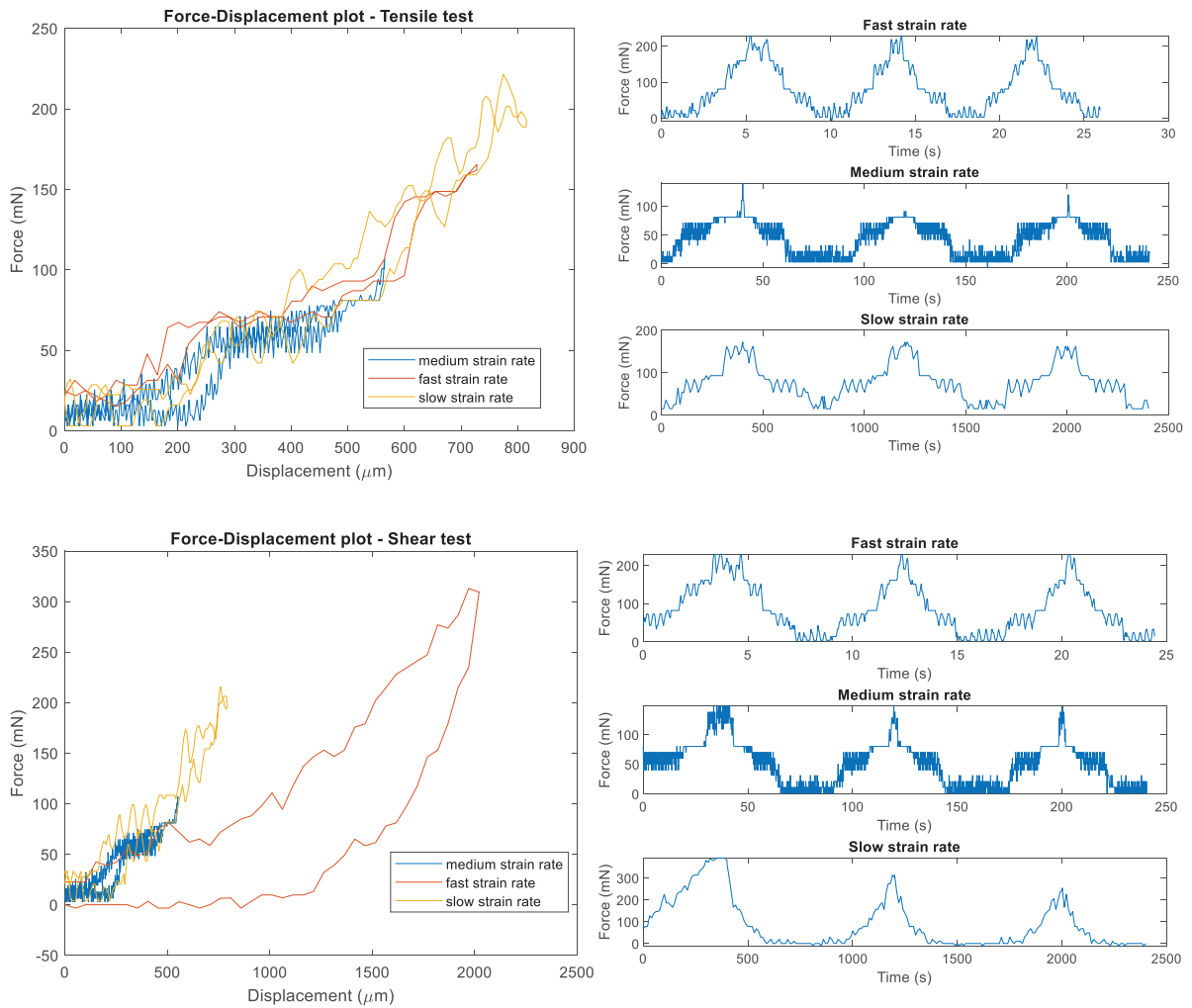


FIGURE 13: MECHANICAL TEST RESULTS FOR TENSILE TESTING, PRESENTED AS A) A FORCE-DISPLACEMENT PLOT AND B) FORCE-TIME PLOTS FOR ALL SESSIONS. SHEAR TEST RESULTS ARE ALSO SHOWN AS C) A FORCE-DISPLACEMENT PLOT AND D) FORCE-TIME PLOTS FOR ALL SESSIONS.

Both medium strain rate sessions show a significant amount of noise. Sample slippage was recorded in shear test at slow strain rate, and a large hysteresis region was recorded for this rate as well. Tensile tests revealed small, but not negligible, hysteresis areas, and similar stiffnesses. Shear test results showed higher stiffnesses for slow and medium strain rates, and a low stiffness for fast strain rate.

Chapter IV: Discussion

1. Identification of EF within areas of interest

Identification of EF network was a challenge, as their relatively small sizes demanded a higher magnification to be visible. Controlling the SEM camera when set at high magnifications to scan the surfaces of all samples was time-consuming. Moreover, regions of interest must occur away from the samples' edges, corresponding to the ILM's location. Edge tears were more prominent than ruptures, possibly due to physical damages caused by sectioning and chemical damages from the alkaline solution.

It was also challenging to identify the lamella-ILM boundaries on SEM. SEM can only produce monochromatic images, and the texture between these areas were similar when under-digested (Figure 14a,b). When samples were placed inside holders after sectioning, they were purposefully arranged so that the direction of the lamellae could be easily identified with the help of the direction marker. Boundaries were recognised as subtle light-coloured ridges (Figure 14c), which, in turn, depended on the contrast of the SEM camera.

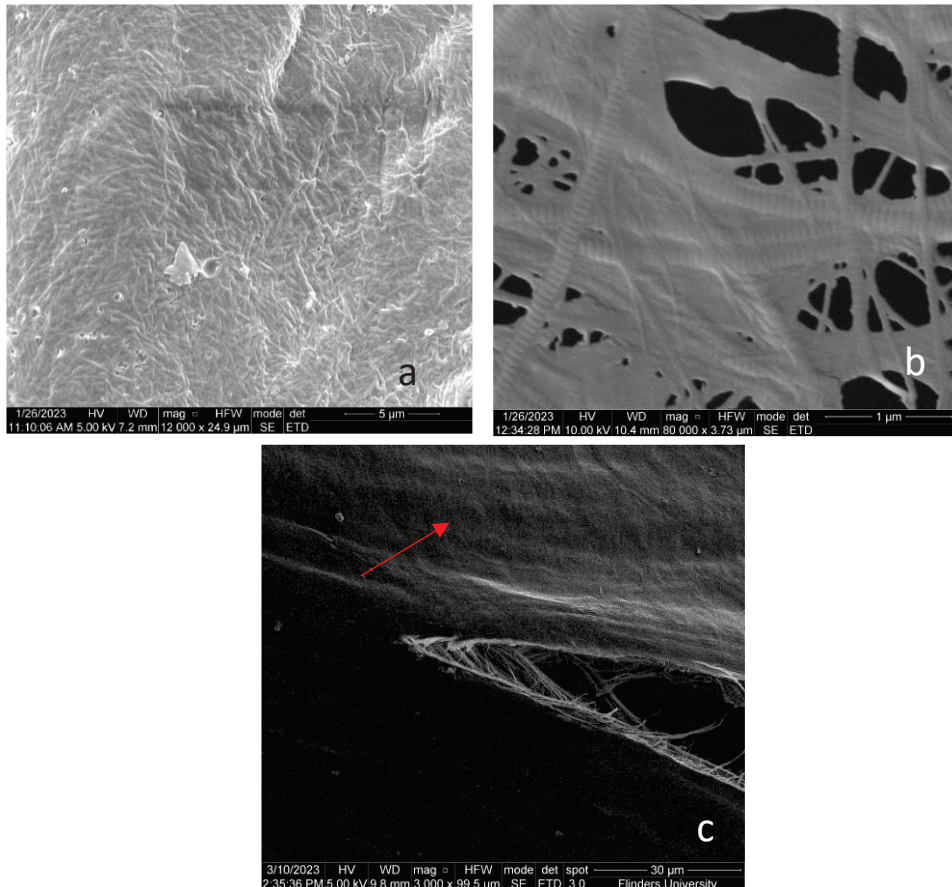


FIGURE 14: UNDIGESTED SURFACE TEXTURE AT A) 12,000 MAGNIFICATION, AND B) 80,000 MAGNIFICATION, SHOWING BANDING IN FIBRES. C) A TEAR, WITH PARALLEL RIDGES POSSIBLY INDICATING LAMELLA-ILM BOUNDARY.

2. Digestion protocol

The protocol testing process did not yield many successful results, which was expected for a trial-and-error procedure. Success could be determined by the number of EF visualised. While specimens were not as vulnerable to human errors thanks to the incorporation of 3D printed apparatuses, a few instances of holders cracking subjected some samples to manual handling, resulting in folding of samples. Folding could potentially obscure some regions from being identified.

Compared to previous attempts (as demonstrated in Figure 15), the obtained images show clearer fibres and in greater numbers. Fibre count was comparable to that of Dr. Tavakoli's ovine ILM results, although the ILM layer was not as clearly defined. This outcome shows a step in the right direction for this project and inspires a starting point for further development.

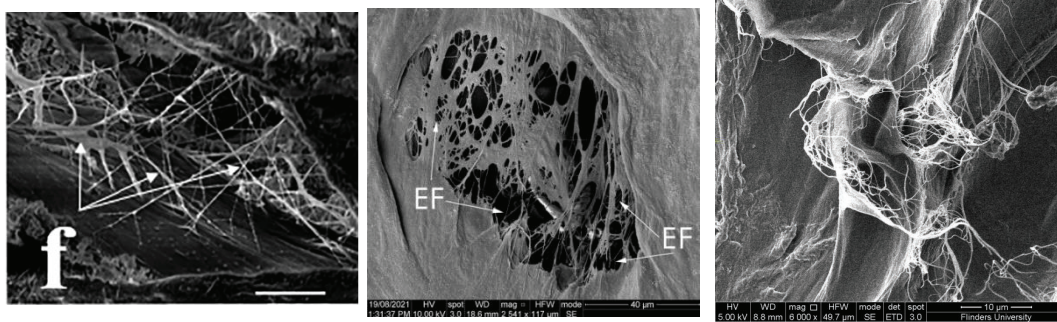


FIGURE 15: COMPARISON BETWEEN DR. TAVAKOLI'S OVINE ILM RESULTS, DANIEL'S HUMAN ILM RESULTS, AND THIS PROJECT'S BEST OUTCOME.

a) Hand microtome sectioning

Freezing and thawing can disrupt the integrity of biological structures. As a result of being transported across different facilities, frozen IVD sections were subjected to a rise in temperature that ice gel packs could not realistically compensate for, thus compromising the quality of the samples. As such, hand microtome sectioning was attempted, with the idea that since the sample preparation location was situated near the digestion site, the samples could be kept fresh and digestion could be carried out immediately without the need for freezing. Difficulties were encountered when trying to make thin cuts using the hand microtome. Tissue O.C.T. compound could not be kept below solidifying threshold throughout the cutting process, even when refreezing was attempted. Liquifying of binding compound resulted in specimens sliding around as the razor blade was pushed across the microtome surface. Thus, only a small number of cuts were deemed successful, and thickness consistency could not be guaranteed.

The slices produced were 0.3 mm and 0.5 mm in thickness, which was way above the minimum thickness the hand microtome could theoretically achieve (10 μm). They were also many times thicker than the slice thickness recommended by Dr. Tavakoli, which was 30 μm . To proceed with these samples would mean that drastically different parameters were required to yield successful results; namely, a much stronger alkaline, longer sonication time, and longer heat treatment duration. It was not within the project's scope to devise a new starting point for these parameters, so the hand microtome method was discontinued in favour of an approach closer to what had been suggested by previous papers.

b) Effects of different parameters on digestion results

i) Molarity and digestion time

Two parameters that determined the quality of results and could be varied from session to session were the molarity of the NaOH solution and the sonication time. They not only affect the degree of digestion, but also the integrity of the sample holder, as shall be discussed later in this paper. The general observation was that higher molarity and longer sonication time would result in a greater level of tissue disruption. Demonstratively, sonicating at 90 minutes and 120 minutes in 0.5M NaOH resulted in decent EF visibility for 30 μm slices, but the best results came from using 1M NaOH while sonicating 50 μm at a longer time. Good results were also found in session #24 where the sonication was only 60 minutes long, but the sample was placed closer to the nozzle. Using the thickness of 50 μm was a step in the right direction, since these slices could hold up in 1M NaOH better than 30 μm slices, leaving more room for experimentation.

Because of time constraints, only 0.5M and 1M were considered, and sonication time was varied between 60 minutes, 90 minutes, 100 minutes, 120 minutes, and 150 minutes. Due to the sensitivity of the protocol, optimal results might be obtained outside of these variations. Doubling the molarity resulted in a more drastic response, as expected, while varying the sonication time seemed to only have noticeable effects around 100 – 120 minutes. The window between under-digestion and complete disintegration was narrow for 1M NaOH, and a sonication time longer than 150 minutes will need to be considered if the molarity of 0.5M is pursued.

ii) Slice thickness

Dr. Tavakoli suggested that a change in sample thickness may have an impact on the protocol's outcome (Javad Tavakoli & John J. Costi, 2018a). For 30 μm samples, total disintegration (N = 4 per session) occurred when sonicating in 1M NaOH at 120 minutes. They were also more susceptible to destruction from other parameters, such as proximity to the nozzle. The chance of dissolution was greatly lowered when working with 50 μm samples; well-digested and under-digested samples could be obtained with higher molarity and sonication time. This observation was relatively consistent throughout different sessions. Meanwhile, little digestion could be detected when using 0.5M NaOH for 30 μm . The number

of tears and holes without visible fibres was also greater. Thus, it can be concluded that 30 μm samples are more susceptible to disintegration than 50 μm , and thicker slices may be better for withstanding the molarity and sonication time required to achieve optimal results. Later sessions thus prioritised the 50 μm thickness. However, this does not rule out the scenario that the optimal results can be achieved when sonicating for longer than 3 hours, or when using a molarity between 0.5M and 1M, but due to time constraints these approaches were not pursued.

A drastic difference in digestion results between 30 μm and 50 μm slices also brings up the possibility of using a slice thickness in between (i.e. 40 μm). This approach can be examined in future research if 50 μm slices continue to yield insufficient results.

iii) Nozzle distance

From Daniel's results, it can be seen that the closer samples are to the nozzle, the more effective the sonication was, while placing the samples further from the nozzle lead to less collagen dissolution. These observations were attempted in sessions #10 and #12, where thoracic samples were used. During session #10, the screws were moved upwards, allowing the sample holder to float at 12 cm from the nozzle tip. The instability of this placement caused the holder to wobble when blasted with sonic waves, which might have contributed to three of the samples' quick disintegration. This approach was not pursued, and instead the nozzle distance was decreased by placing the beaker on a low platform.

The change in nozzle distance yielded inconsistent results. Better visualisation was achieved after the 60-minute session (#24) compared to the 90- or 120-minute sessions (#25 and #26), with #26 resulting in disintegration. Taking into account accidents such as sample holders cracking, it can be suggested that a closer distance does affect collagen digestion, just not in a predictable pattern. One possible explanation is that by bringing the holder closer to the nozzle, the ultrasonic wave pattern might have been less widespread, thus areas at the centre of the holder were most affected (Figure 16).

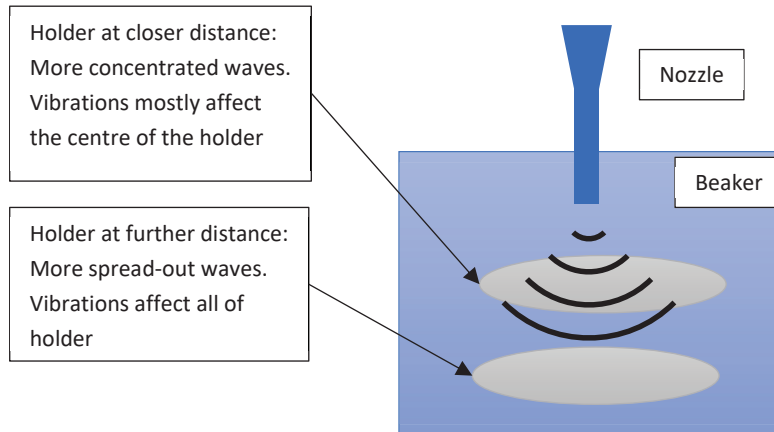


FIGURE 16: POSSIBLE EXPLANATION FOR THE INTERACTION BETWEEN ULTRASONIC WAVES AND SAMPLE HOLDERS AT DIFFERENT DISTANCES TO NOZZLE.

iv) FSU location

Thoracic samples seemed to be more prone to disintegration. As many problems were encountered during these sessions, however, it was unclear if the change in FSU location definitively affected the digestion outcome. Thoracic IVDs theoretically withstand less loading compared to lumbar IVDs; study shows that they have lower disc height and shape compared to lumbar discs, but their fibre content should not greatly differ (Pooni et al., 1986). To ensure that the results are consistent with the goals of the study, only lower lumbar discs should be used.

v) Sectioning orientation

Dr. Tavakoli's results (J. Tavakoli & J. J. Costi, 2018) suggested an improvement in EF visibility when applying oblique cuts on disc sections during microtome cutting. Similar oblique cuts were attempted; however, as the cryostat microtome's tilted platform was not fully stable during sectioning, consistency in slice thickness could be a concern. There was no perceived unevenness across the sample surface, but full digestion was consistently more difficult to reach when working with obliquely cut slices. This could be due to the aforementioned inconsistency that might have left some areas more resistant to alkaline digestion. More testing should be done to fully investigate the effects of cutting orientation.

vi) Heat treatment

The heat treatment stage was only altered in two sessions, #32 and #33, both resulting in little improvement in EF visualisation. Increasing the temperature caused the sample holder to

warp, rendering it unfit for SEM imaging. Dr. Tavakoli suggested a longer heat treatment duration for human samples in contrast to ovine samples, but there seems to be little improvement in terms of effectiveness when the duration was increased during session #33. This could be explained by considering the purpose of heat treatment, which is removing loose collagen fibres. In order for this stage to be effective, undesired protein should already be loosened – an outcome that can be achieved through sonication. That being the case, the sample size was still small (N = 8), so more testing is needed to draw a conclusion.

vii) Other factors

Samples used throughout the project were cut from different AF regions, barring posterior and posterolateral. The IVD is heterogeneous, in that the fibre arrangement and fibre count are different between regions (Holzapfel et al., 2005). The difference, however, is near-negligible between lateral, anterolateral, and anterior AF. There was little evidence that this spatial variation played a role in the digestion process, although a further look into this factor is encouraged.

So far, no session was able to produce good results for all 4 samples. This inconsistency could be due to the non-uniform pattern of ultrasonic blasts as discussed in part iii). It could also be due to the position of the sample holder inside the beaker. There were instances where holders were pushed around during sonication, and in theory this could cause some samples to be more affected than the rest. A solution to this would be to design a stand that keeps the holders stationary, and possibly a larger sample holder that allows samples to be placed further apart.

c) SEM imaging quality

The scanning electron microscope uses an electron beam to scan the surface of the target and is capable of very high magnification. One common source of SEM artifact is charge-up noise, which is produced when the specimen isn't conductive enough. Beam electrons cannot be transferred through a non-conductive material's surface, so they start to accumulate within the specimen. Excessive electrons are backscattered and result in noisy images. Exposure to non-conductive materials also cause drifting, making focusing and navigating challenging. Biological samples are non-conductive, and thus they require to be coated before being imaged. For the first few sessions, sample holders were coated on one side with a 5 nm

layer of Pt. The images obtained were heavily distorted. Drifting also inhibited focusing and prevented high quality images from being developed.

This problem was identified as a result of the sample holders' usage. The holders were fabricated using PLA filaments, which is a non-conductive material. When placed inside the SEM's vacuum chamber, they would not have full contact with the metal platform, exposing uncoated parts of the samples to the electron beam. This could be avoided by increasing the layer thickness to 10 nm and coating both sides of the sample. Visibility notably improved using this method, although small amounts of artifact still occurred at higher magnifications (above 12,000).

d) Effects of the digestion process on 3D printed apparatuses

For the first 9 sessions, sample holders with the thickness of 1 mm were used, and damages could be detected when sonicated for higher molarities at longer time. NaOH is a highly corrosive substance, thus it can cause breakage to the holders' and even the stand's structure. Repeated usage can also result in a decrease in material integrity. In some sessions, cracks were found in the top meshes of sample holders. In others, breakage of the holder's top half caused samples to be extruded. Most escaped samples could be recovered from the beaker after sonication; however, forceps handling caused them to become folded and thus, difficult to be properly imaged. Samples extruded halfway through the sonication process can also fall to the bottom of the beaker, changing the distance between them and the nozzle, resulting in inconsistencies across samples of the same holder. These samples were also subjected to turbulence and experienced mechanical damages, affecting their integrity.

Warping of sample holders was detected during heat treatment at the temperature of 80°C. This caused the holders to be ineligible for SEM imaging, and so samples had to be transferred to an intact holder. While the approach was not attempted during this study, heat warping also poses a challenge for the hot alkaline method.

There were several instances where the central pole of the stand broke off either during or before sonication. This was understandable as stands were reused for multiple sessions; the screws were originally tightened around the pole which contributed to it breaking off under the vibrations and the corrosive effect of the solution. In later sessions, screws were placed on top of the holder.

This shows that PLA is not the most suitable material to print the models used for this protocol. It has low heat resistance, with a heat distortion temperature of around 55°C (Yang et al., 2016). Its chemical resistance is decent, yet prolonged and repeated exposure to strong alkaline can greatly compromise the integrity of the models, leading to unwanted breakage during the protocol. Moreover, delicate features such as the meshes are crucial to the sample holder's function. An increase in mesh width would result in the sonic waves not properly penetrating the contained samples. Ideally, these apparatuses should be printed using a more durable material with high heat and chemical resistance. Density should also be considered to eliminate the use of screws.

e) Mechanical testing

Digested samples were more vulnerable to tearing compared to intact samples, so extra care was taken while preparing for mechanical testing. Most failures came from transporting and loading sample into the test equipment after sandpaper pieces had been attached. To prevent as much stress exerted on samples as possible, samples would be wedged between glass slide and held in place, while actuators were adjusted using the software. This technique led to a notable decrease in sample failure.

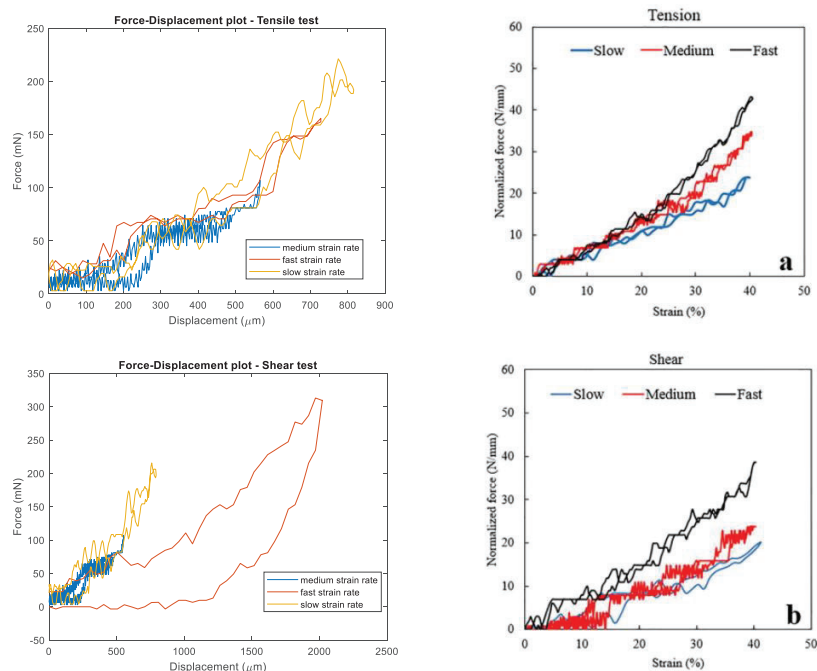


FIGURE 17: QUALITATIVE COMPARISON TO DIGEST ILM'S BEHAVIOUR IN OVINE DISCS. LEFT SIDE: PARTIALLY DIGESTED HUMAN ILM. RIGHT SIDE: NORMALISED DIGESTED OVINE ILM RESULTS (JAVAD TAVAKOLI & JOHN J. COSTI, 2018B). BOTH WERE TESTED USING THE SAME STRAIN RATES.

It is hypothesized that the EF network exhibits elastic behaviour, which in turn means that a digested ILM sample would show an increase in elastic response, and decrease in hysteresis region, when tested. The responses obtained, as shown in Figure 17 in comparison with previous ovine ILM results by Dr. Tavakoli, still had large hysteresis regions, particularly during shear test sessions, and at a medium strain rate for both tensile and shear tests. No clear distinction in stiffness was identified between strain rates. This was expected, as test conditions were not desirable due to a number of factors. First, the ILM samples were not fully digested, as the protocol had not been developed yet, so remaining collagen fibres may have contributed to the viscoelastic behaviour. Slight sample slippage was also the cause of incorrect stress readings. It should also be noted that the sample showed signs of fatigue during the shear test at slow strain rate.

Load cell readings were particularly problematic during tests at medium strain rate. At certain points, readings became much less sensitive and started jumping between values, resulting in extremely noisy graphs. These errors also led to preloading not being applied properly, as a decrease in sensitivity around the 50 Nm – 100 Nm point led to samples being overloaded and torn.

Chapter V: Future Work

A sample thickness of 50 μm is recommended for future sessions, so that longer durations can be applied with a lower risk of disintegration. Better results were obtained when sonicating for longer than 90 minutes using 1M of NaOH. It is advised that further attempts can tackle durations of 130 minutes, 140 minutes, and above 150 minutes, provided that an improvement in sample holder durability was made. 0.5 NaOH can potentially provide good results at a longer sonication time, proposedly 150 – 200 minutes. Furthermore, due to the sensitive nature of this procedure, smaller increments in duration can also be implemented (i.e. sonicating for 120 minutes in one session, then 125 minutes in the next).

Molarity can also be varied, although care should be taken so that damages to materials due to corrosion are minimised. A suggestion would be using molarities between 0.5M and 1M, with possible increments of 0.1M between sessions. For comparison's sake, a constant sonication time should be followed when molarity is varied (proposedly 120 – 150 minutes). Using higher than 1M is not encouraged as samples can easily be compromised.

More testing is needed to determine the effects of oblique cuts and heat treatment duration on EF visualisation. If no clear distinction is observed, a better method should be determined to obtain oblique cuts, as the Leica microtome does not have features that allow accurate angled sectioning. An angle of 30°, as proposed by Dr. Tavakoli, should be attempted if possible.

The heat treatment stage can be varied, although drastic changes can lead to destruction of the sample holder. A heating duration of 20 – 30 minutes can be attempted, and if holder durability is guaranteed, temperature can be increased to 80°C.

The regions of IVD from which samples are taken should be accounted for in future attempts to ensure consistency. Due to the thickness of their AF, anterior and anterolateral segments are easier for mechanical testing, so these regions should be aimed for in further tests. Posterolateral and posterior regions are also worth investigating, due to their vulnerability to degeneration compared to anterior regions, although they should only be pursued if satisfactory results can be achieved using anterior regions.

Variation of nozzle distance is worth investigating if the pattern of ultrasonic waves expelled from the sonicator's nozzle is known. Placing sample holder further from the nozzle may not necessarily mean less digestion is expected, so this could be an approach worth attempting. A new stand design should be derived to allow for sample holder to be kept at the bottom of the beaker.

Once a decent isolation procedure is achieved, mechanical testing can be carried out comfortably. Sample preparation and handling techniques developed during this project are largely sufficient, with the exception of preloading. Samples should be properly preloaded in the future, and tests should only be carried out if a load of 100 Nm is reached. While the techniques themselves are adequate, accidents can still happen, resulting in sample slippage, failures, etc. Glue should be given enough time to dry, and an appropriate amount should be applied to avoid flooding of the region of interest. Calibration of test equipment should be done to ensure accuracy.

Chapter VI: Conclusion

Research into the mechanical properties of elastic fibres provides insight into the behaviour of the annulus fibrosus and the intervertebral disc. However, a method to isolate elastic fibres has not been concluded. The digestion protocol is difficult to perfect, due to various factors that can affect the outcome. Working with thin, delicate samples is challenging, so the incorporation of sample holders and stands massively improves the procedure; however, it also poses some challenges in acquiring a good final outcome (such as SEM image quality). Varying the duration of sonication and the molarity of NaOH solution is a good starting point, however other factors should be accounted for.

Time constraint was a major challenge in this project. Reliability is an important goal, and it would require multiple repeats of the same protocol, not to mention unwanted factors that may diversify the final results. The digestion process is also lengthy, reaching up to 20 hours per session.

The obtained results show great improvement in EF visualisation compared to previous attempts. Further optimisation is needed before the method can be reliably applied. Better results were achieved when a higher molarity (1M) was used, and generally for a longer sonication time (above 90 minutes). A decrease in nozzle distance also led to better digestion in some instances, however this effect was not reliable. More testing is needed to optimise the digestion method.

Bibliography

- Adams, M. A., & Dolan, P. (2015). 10 - Biomechanics of the spine. In M. C. Hochberg, A. J. Silman, J. S. Smolen, M. E. Weinblatt, & M. H. Weisman (Eds.), *Rheumatology (Sixth Edition)* (pp. 72-79). Mosby. <https://doi.org/https://doi.org/10.1016/B978-0-323-09138-1.00010-3>
- Adams, M. A., & Roughley, P. J. (2006). What is Intervertebral Disc Degeneration, and What Causes It? *Spine*, 31(18).
https://journals.lww.com/spinejournal/Fulltext/2006/08150/What_is_Intervertebral_Disc_Degeneration,_and_What.24.aspx
- Alonso, F., & Hart, D. J. (2014). Intervertebral Disk. In M. J. Aminoff & R. B. Daroff (Eds.), *Encyclopedia of the Neurological Sciences (Second Edition)* (pp. 724-729). Academic Press. <https://doi.org/https://doi.org/10.1016/B978-0-12-385157-4.01154-4>
- Azhim, A., Yamagami, K., Muramatsu, K., Morimoto, Y., Furukawa, K. S., Tanaka, M., Fukui, Y., & Ushida, T. (2013, 2013//). The Use of Sonication Treatment to Completely Decellularize Aorta Tissue. World Congress on Medical Physics and Biomedical Engineering May 26-31, 2012, Beijing, China, Berlin, Heidelberg.
- Baldit, A. (2018). 11 - Micromechanics of the Intervertebral Disk. In J.-F. Ganghoffer (Ed.), *Multiscale Biomechanics* (pp. 455-467). Elsevier. <https://doi.org/https://doi.org/10.1016/B978-1-78548-208-3.50011-3>
- Baldoni, M., & Gu, W. (2019). Effect of fixed charge density on water content of IVD during bed rest: A numerical analysis. *Med Eng Phys*, 70, 72-77.
<https://doi.org/10.1016/j.medengphy.2019.06.011>
- Buchbinder, R., van Tulder, M., Öberg, B., Costa, L. M., Woolf, A., Schoene, M., Croft, P., Buchbinder, R., Hartvigsen, J., Cherkin, D., Foster, N. E., Maher, C. G., Underwood, M., van Tulder, M., Anema, J. R., Chou, R., Cohen, S. P., Menezes Costa, L., Croft, P., . . . Woolf, A. (2018). Low back pain: a call for action. *The Lancet*, 391(10137), 2384-2388.
[https://doi.org/https://doi.org/10.1016/S0140-6736\(18\)30488-4](https://doi.org/https://doi.org/10.1016/S0140-6736(18)30488-4)
- Daamen, W. F., Hafmans, T., Veerkamp, J. H., & van Kuppevelt, T. H. (2005). Isolation of intact elastin fibers devoid of microfibrils. *Tissue Eng*, 11(7-8), 1168-1176.
<https://doi.org/10.1089/ten.2005.11.1168>
- Damian, H., Lyn, M., Peter, B., Fiona, B., Anthony, W., Christopher, B., Gail, W., Emma, S., Theo, V., Jan, B., Chris, M., Roy, B., & Rachelle, B. (2014). The global burden of low back pain: estimates from the Global Burden of Disease 2010 study. *Annals of the Rheumatic Diseases*, 73(6), 968. <https://doi.org/10.1136/annrheumdis-2013-204428>
- Fletcher, M. M., Bruce, A. W., Hsiu-Mei, W., & David, M. Y. (2002). Serial MR Imaging of Annular Tears in Lumbar Intervertebral Disks. *American Journal of Neuroradiology*, 23(7), 1105.
<http://www.ajnr.org/content/23/7/1105.abstract>
- Gotte, L., Stern, P., Elsdén, D. F., & Partridge, S. M. (1963). The chemistry of connective tissues. 8. The composition of elastin from three bovine tissues. *Biochem J*, 87(2), 344-351.
<https://doi.org/10.1042/bj0870344>
- Gregory, D. E., Bae, W. C., Sah, R. L., & Masuda, K. (2012). Anular delamination strength of human lumbar intervertebral disc. *European Spine Journal*, 21(9), 1716-1723.
<https://doi.org/10.1007/s00586-012-2308-x>
- Guterl, C. C., See, E. Y., Blanquer, S. B., Pandit, A., Ferguson, S. J., Benneker, L. M., Grijpma, D. W., Sakai, D., Eglín, D., Alini, M., Iatridis, J. C., & Grad, S. (2013). Challenges and strategies in the repair of ruptured annulus fibrosus. *Eur Cell Mater*, 25, 1-21.
<https://doi.org/10.22203/ecm.v025a01>
- Gylseth, B., Baunan, R. H., & Overaa, L. (1982). Analysis of Fibres in Human Lung Tissue. *British Journal of Industrial Medicine*, 39(2), 191-195. <http://www.jstor.org/stable/27723607>

- Holzapfel, G. A., Schulze-Bauer, C. A. J., Feigl, G., & Regitnig, P. (2005). Single lamellar mechanics of the human lumbar annulus fibrosus. *Biomechanics and Modeling in Mechanobiology*, 3(3), 125-140. <https://doi.org/10.1007/s10237-004-0053-8>
- Hoy, D., Brooks, P., Blyth, F., & Buchbinder, R. (2010). The Epidemiology of low back pain. *Best Practice & Research Clinical Rheumatology*, 24(6), 769-781. <https://doi.org/https://doi.org/10.1016/j.berh.2010.10.002>
- Inoue, H., & Takeda, T. (1975). Three-dimensional observation of collagen framework of lumbar intervertebral discs. *Acta Orthop Scand*, 46(6), 949-956. <https://doi.org/10.3109/17453677508989283>
- John, R., & Thomas, J. (1972). Chemical compositions of elastins isolated from aortas and pulmonary tissues of humans of different ages. *Biochem J*, 127(1), 261-269. <https://doi.org/10.1042/bj1270261>
- Keeley, F. W., & Partridge, S. M. (1974). Amino acid composition and calcification of human aortic elastin. *Atherosclerosis*, 19(2), 287-296. [https://doi.org/https://doi.org/10.1016/0021-9150\(74\)90063-X](https://doi.org/https://doi.org/10.1016/0021-9150(74)90063-X)
- Kielty, C. M., Sherratt, M. J., & Shuttleworth, C. A. (2002). Elastic fibres. *J Cell Sci*, 115(Pt 14), 2817-2828. <https://doi.org/10.1242/jcs.115.14.2817>
- Lannoy, M., Slove, S., & Jacob, M. P. (2014). The function of elastic fibers in the arteries: Beyond elasticity. *Pathologie Biologie*, 62(2), 79-83. <https://doi.org/https://doi.org/10.1016/j.patbio.2014.02.011>
- Lin, C. H., Hsia, K., Su, C. K., Chen, C. C., Yeh, C. C., Ma, H., & Lu, J. H. (2021). Sonication-Assisted Method for Decellularization of Human Umbilical Artery for Small-Caliber Vascular Tissue Engineering. *Polymers (Basel)*, 13(11). <https://doi.org/10.3390/polym13111699>
- Livshits, G., Popham, M., Malkin, I., Sambrook, P. N., Macgregor, A. J., Spector, T., & Williams, F. M. (2011). Lumbar disc degeneration and genetic factors are the main risk factors for low back pain in women: the UK Twin Spine Study. *Ann Rheum Dis*, 70(10), 1740-1745. <https://doi.org/10.1136/ard.2010.137836>
- Long, J. L., & Tranquillo, R. T. (2003). Elastic fiber production in cardiovascular tissue-equivalents. *Matrix Biology*, 22(4), 339-350. [https://doi.org/https://doi.org/10.1016/S0945-053X\(03\)00052-0](https://doi.org/https://doi.org/10.1016/S0945-053X(03)00052-0)
- Marcolongo, M., Sarkar, S., & Ganesh, N. (2017). 7.11 Trends in Materials for Spine Surgery. In P. Ducheyne (Ed.), *Comprehensive Biomaterials II* (pp. 175-198). Elsevier. <https://doi.org/https://doi.org/10.1016/B978-0-08-100691-7.00269-X>
- Mengoni, M., Luxmoore, B. J., Wijayathunga, V. N., Jones, A. C., Broom, N. D., & Wilcox, R. K. (2015). Derivation of inter-lamellar behaviour of the intervertebral disc annulus. *Journal of the Mechanical Behavior of Biomedical Materials*, 48, 164-172. <https://doi.org/https://doi.org/10.1016/j.jmbbm.2015.03.028>
- Nepomuceno, M. R., & Turra, C. M. (2015). Trends in healthy life expectancy among older Brazilian women between 1998 and 2008. *Rev Saude Publica*, 49, 1. <https://doi.org/10.1590/s0034-8910.2015049005472>
- Pezowicz, C. A., Robertson, P. A., & Broom, N. D. (2006). The structural basis of interlamellar cohesion in the intervertebral disc wall. *J Anat*, 208(3), 317-330. <https://doi.org/10.1111/j.1469-7580.2006.00536.x>
- Pierce, J. A., & Ebert, R. V. (1965). Fibrous Network of the Lung and its Change with Age. *Thorax vol. 20*, 5(0040-6376 (Print)).
- Pooni, J. S., Hukins, D. W., Harris, P. F., Hilton, R. C., & Davies, K. E. (1986). Comparison of the structure of human intervertebral discs in the cervical, thoracic and lumbar regions of the spine. *Surg Radiol Anat*, 8(3), 175-182. <https://doi.org/10.1007/bf02427846>
- Raj, P. P. (2008). Intervertebral disc: anatomy-physiology-pathophysiology-treatment. *Pain Pract*, 8(1), 18-44. <https://doi.org/10.1111/j.1533-2500.2007.00171.x>

- Ross, R., & Bornstein, P. (1969). THE ELASTIC FIBER : I. The Separation and Partial Characterization of its Macromolecular Components. *Journal of Cell Biology*, 40(2), 366-381.
<https://doi.org/10.1083/jcb.40.2.366>
- Smith, L. J., & Fazzalari, N. L. (2009). The elastic fibre network of the human lumbar annulus fibrosus: architecture, mechanical function and potential role in the progression of intervertebral disc degeneration. *Eur Spine J*, 18(4), 439-448. <https://doi.org/10.1007/s00586-009-0918-8>
- Tavakoli, J., & Costi, J. J. (2018a). A method for visualization and isolation of elastic fibres in annulus fibrosus of the disc. *Materials Science and Engineering: C*, 93, 299-304.
<https://doi.org/https://doi.org/10.1016/j.msec.2018.08.007>
- Tavakoli, J., & Costi, J. J. (2018b). New insights into the viscoelastic and failure mechanical properties of the elastic fiber network of the inter-lamellar matrix in the annulus fibrosus of the disc. *Acta Biomaterialia*, 77, 292-300.
<https://doi.org/https://doi.org/10.1016/j.actbio.2018.07.023>
- Tavakoli, J., & Costi, J. J. (2018). Ultrastructural organization of elastic fibres in the partition boundaries of the annulus fibrosus within the intervertebral disc. *Acta Biomaterialia*, 68, 67-77. <https://doi.org/https://doi.org/10.1016/j.actbio.2017.12.017>
- Tavakoli, J., Elliott, D. M., & Costi, J. J. (2016). Structure and mechanical function of the inter-lamellar matrix of the annulus fibrosus in the disc. *J Orthop Res*, 34(8), 1307-1315.
<https://doi.org/10.1002/jor.23306>
- Tavakoli, J., Elliott, D. M., & Costi, J. J. (2017). The ultra-structural organization of the elastic network in the intra- and inter-lamellar matrix of the intervertebral disc. *Acta Biomaterialia*, 58, 269-277. <https://doi.org/https://doi.org/10.1016/j.actbio.2017.05.036>
- Tenny, S., & Gillis, C. C. (2023). Annular Disc Tear. In *StatPearls*. StatPearls Publishing
- Copyright © 2023, StatPearls Publishing LLC.
- Walker, B. F., Muller, R., & Grant, W. D. (2004). Low Back Pain in Australian Adults. Prevalence and Associated Disability. *Journal of Manipulative and Physiological Therapeutics*, 27(4), 238-244.
<https://doi.org/https://doi.org/10.1016/j.jmpt.2004.02.002>
- Yang, Y., Zhang, L., Xiong, Z., Tang, Z., Zhang, R., & Zhu, J. (2016). Research progress in the heat resistance, toughening and filling modification of PLA. *Science China Chemistry*, 59(11), 1355-1368. <https://doi.org/10.1007/s11426-016-0222-7>
- Yu, J., Winlove, P. C., Roberts, S., & Urban, J. P. (2002). Elastic fibre organization in the intervertebral discs of the bovine tail. *J Anat*, 201(6), 465-475. <https://doi.org/10.1046/j.1469-7580.2002.00111.x>

Appendices

Methodology

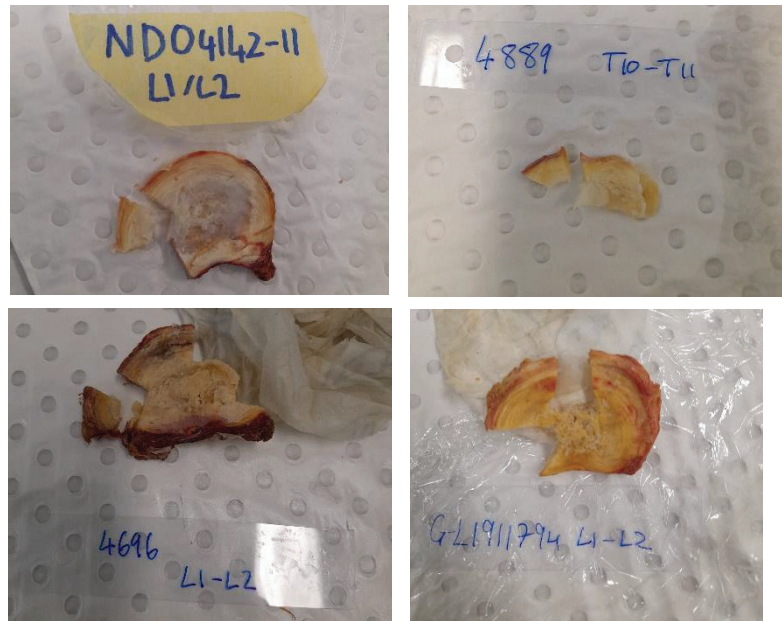


FIGURE 18: SECTIONING OF VARIOUS IVDS.



FIGURE 19: HAND MICROTOME SECTIONED SLICES.



FIGURE 20: ANGLED PLATFORM FOR OBLIQUE CUTTING.



FIGURE 21: A PIECE OF PARTIALLY DIGESTED SAMPLE. THE ILM IS LESS DEFINED, THOUGH STILL VISIBLE.

Results

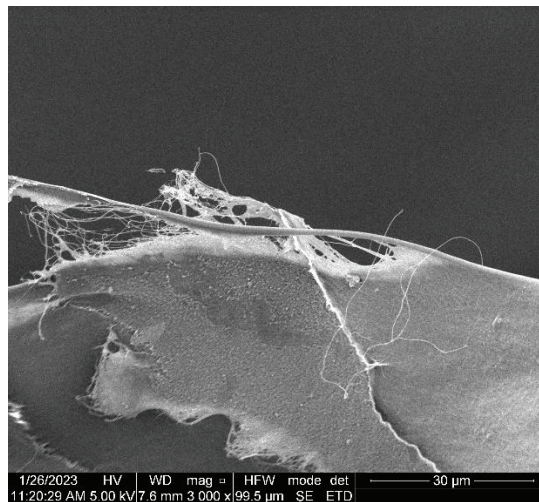


FIGURE 22: SESSION #1

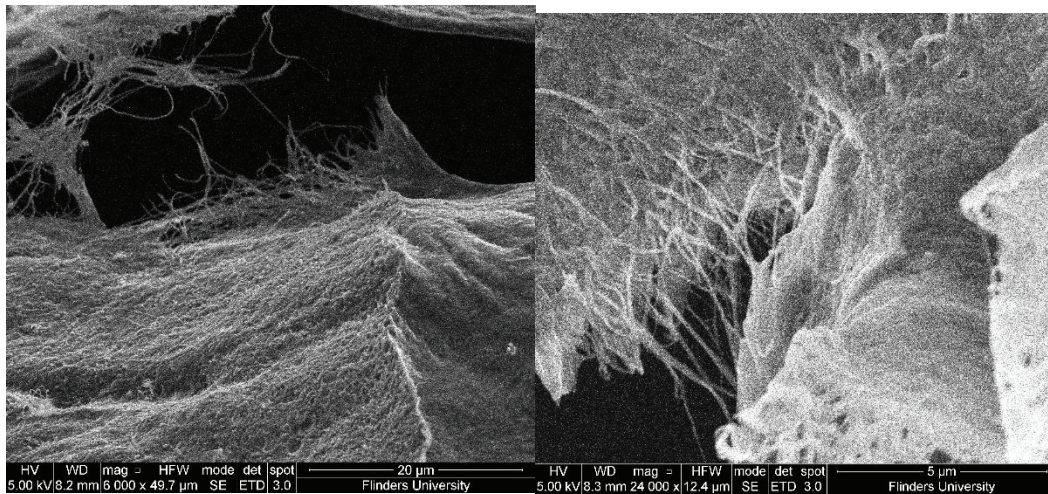


FIGURE 23: SESSION #4

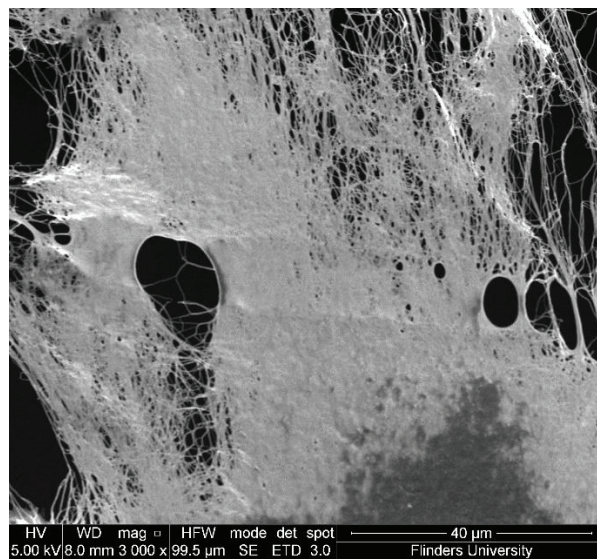


FIGURE 24: SESSION #6

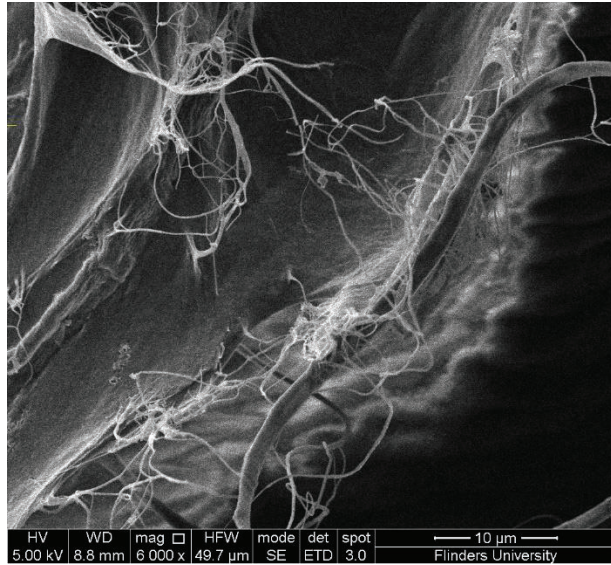


FIGURE 25: SESSION #7

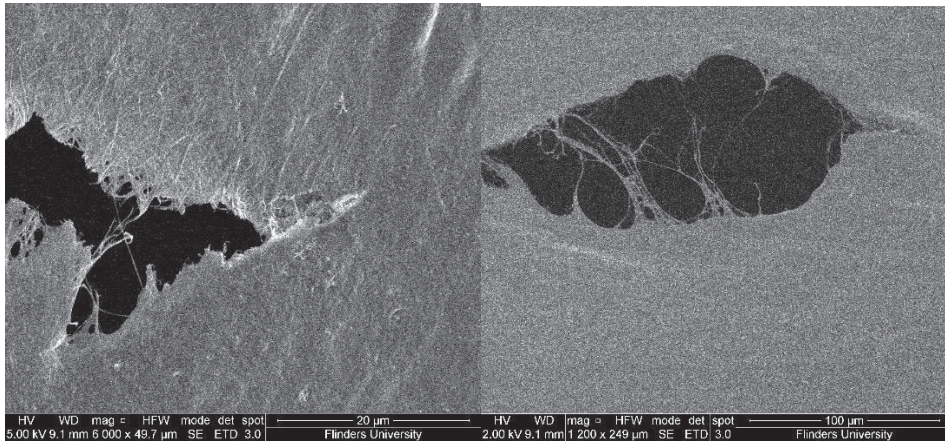


FIGURE 26: SESSION #9

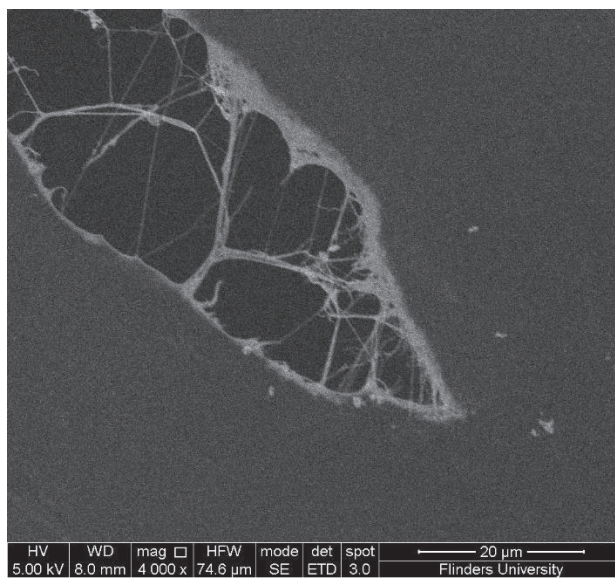


FIGURE 27: SESSION 11

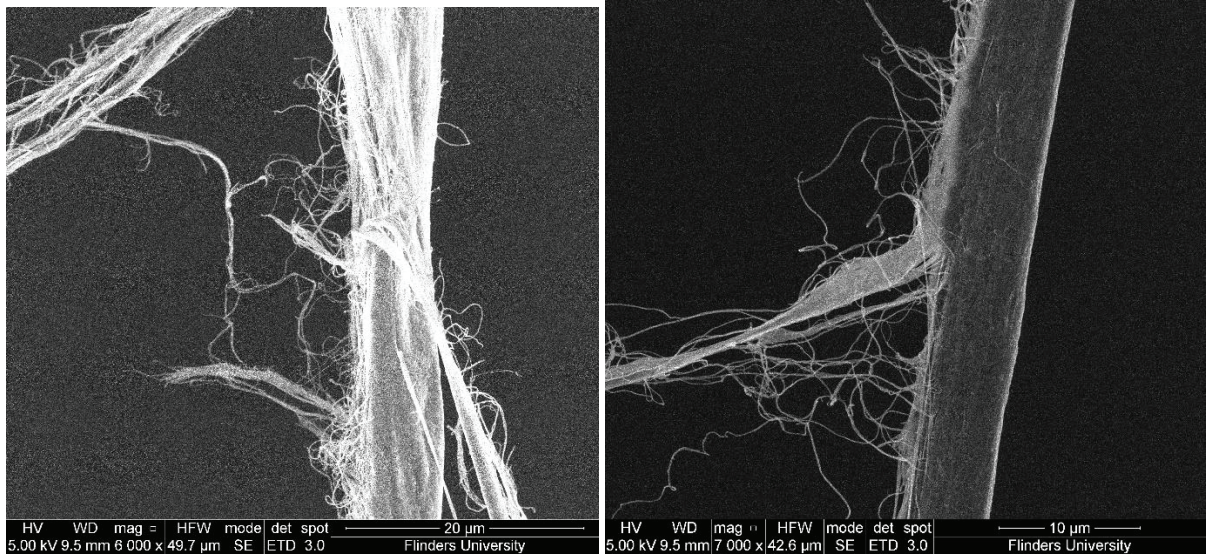


FIGURE 28: SESSION #15

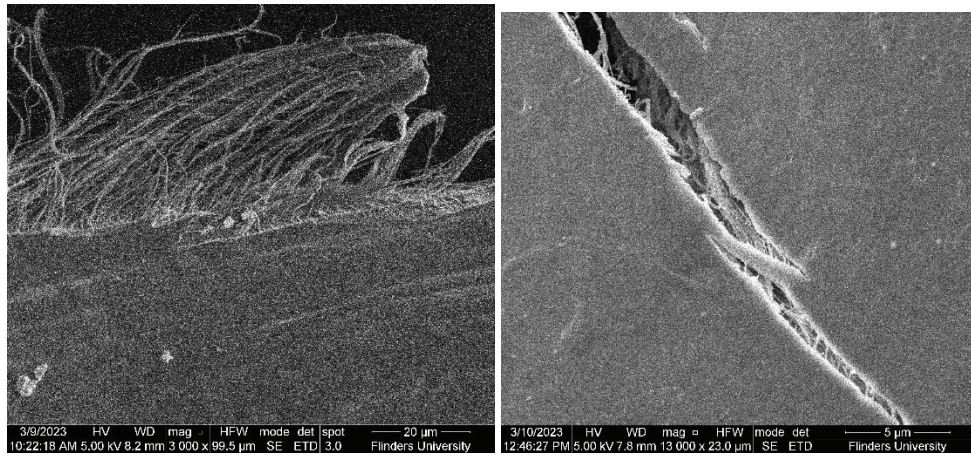


FIGURE 29: SESSION #22 AND #23

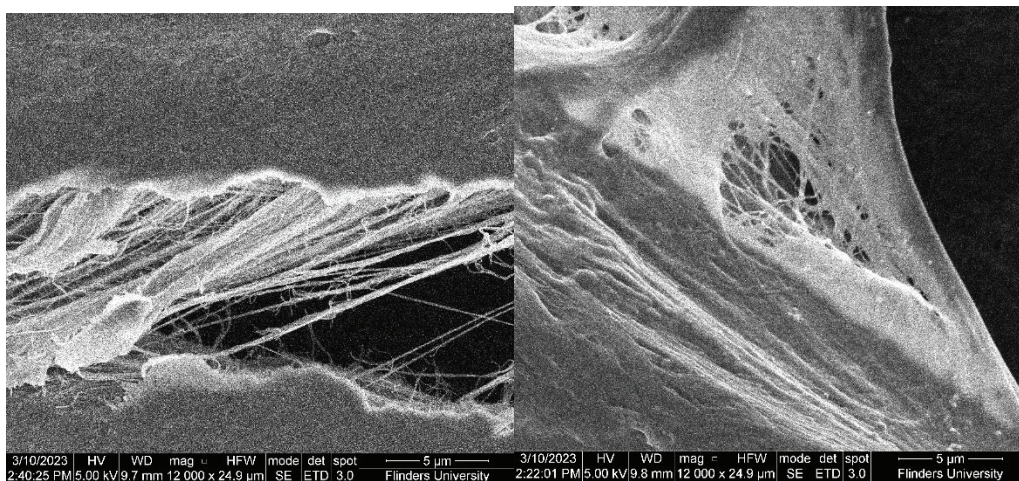


FIGURE 30: SESSION #24

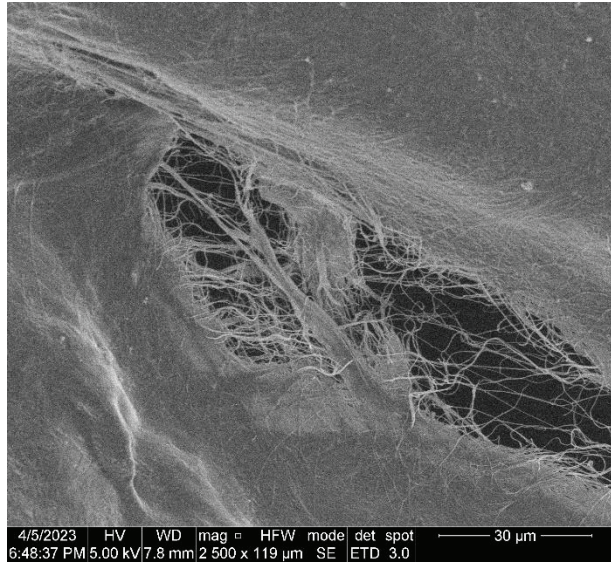


FIGURE 31: SESSION #31